NATIONAL ADVISORY COMMITTEE FOR AERONAUTICS

WARTIME REPORT

ORIGINALLY ISSUED

May 1945 as
Memorandum Report L5D27a

WIND-TUNNEL TESTS OF THE 0.15-SCALE POWERED MODEL

OF THE FLEETWINGS XBTK-1 AIRPLANE

LONGITUDINAL STABILITY AND CONTROL

By Joseph Weil and Rebecca I. Boykin

Langley Memorial Aeronautical Laboratory
Langley Field, Va.

NACA

WASHINGTON

MR No. L5D27a

NATIONAL ADVISORY COMMITTEE FOR AERONAUTICS

MEMORANDUM REPORT

for the

Bureau of Aeronautics, Navy Department

WIND-TUNNEL TESTS OF THE 0.15-SCALE POWERED MODEL

OF THE FLEETWINGS XBTK-1 AIRPLANE

LONGITUDINAL STABILITY AND CONTROL

By Joseph Weil and Rebecca I. Boykin

SUMMARY

An investigation was undertaken to determine the probable static stability and control characteristics of the XBTK-1 airplane. Data from which these character- istics can be determined were obtained from tests of a 0.15-scale powered model in the Langley 7- by 10-foot tunnel.

The results of that part of the investigation which deals specifically with static longitudinal stability and control and stall characteristics are presented in this paper.

The longitudinal stability will probably be satis- factory for all contemplated flight conditions at the rearmost center-of-gravity location with the elevator fixed and free. Power effects were small.

Sufficient elevator control will be available to trim in any flight condition away from the ground. The stick forces may be light if the spring stiffness presently contemplated is used.

Increasing the slotted flap deflection above $30°$ increased $C_{L_{max}}$ only slightly.

Stalling characteristics will probably be satis- factory. In general, stall started at the wing fold line

and spread inboard faster than toward the tip. Power
delayed the stall over portions of the wing immersed in
the slipstream. The presence of the fuel tank, radar,
and wing guns did not appreciably affect the stall trends.

INTRODUCTION

At the request of the Bureau of Aeronautics, Navy
Department, a series of wind-tunnel tests was made in
the Langley 7- by 10-foot tunnel of the Fleetwings
XBTK-1 model (0.15 scale) with power. In addition,
tests were made in the Langley 4- by 6-foot tunnel in
order to determine isolated horizontal-tail charac-
teristics.

The objective of these tests was to determine the
complete stability and control characteristics of the
model and provide data from which the flying qualities
of the airplane could be estimated. The information
thus obtained can be used to ascertain the amount and
extent of modifications necessary to insure satisfactory
handling qualities of the contemplated airplane.

The present report includes the results of the
investigation of the longitudinal stability and control
characteristics of the model. Photographs of tuft
surveys made to determine the stall progression for
various model conditions are also presented.

COEFFICIENTS AND SYMBOLS

The results of the tests are presented as standard
NACA coefficients of forces and moments. Pitching-
moment coefficients are given about the center-of-gravity
location shown in figure 1 (25.6 percent of the mean
aerodynamic chord). The data are referred to a system
of axes originating at the center of gravity in which
the Z axis is in the plane of symmetry and perpendicular
to the relative wind, the X axis is in the plane of
symmetry, and perpendicular to the Z axis, and the
Y axis is perpendicular to the plane of symmetry.

The coefficients and symbols are defined as follows:

C_L lift coefficient (Z/qS)

C_{L_t} tail-lift coefficient $(Tail\ lift/qS_t)$

C_{D_R} resultant-drag coefficient (X/qS)

C_m pitching-moment coefficient (M/qSc)

C_{h_e} elevator hinge-moment coefficient $(H/qb_e\bar{c}_e^2)$

T_c' effective thrust coefficient (T_e/qS)

nD/V propeller diameter-advance ratio

Q_c torque coefficient $(Q/\rho V^2 D^3)$

η propulsive efficiency $(T_e V/2\pi nQ)$

where the quantities are defined below

Z force along Z axis, positive when directed
             upward, pounds

X force along X axis, positive when directed
             backward, pounds

M moment about Y axis, pound-feet

H_e elevator hinge moment, pound-feet

T_e effective thrust, pounds

Q torque, pound-feet

q dynamic pressure $(\rho V^2/2)$, pounds per square
             foot

S wing area (8.55 square feet on model)

S_t horizontal-tail area (1.80 square feet on model)

c wing mean aerodynamic chord (1.22 feet on model)

$\bar{c}_e$ root mean square chord of elevator behind hinge
             line (0.191 foot on model)

b_w wing span (7.30 feet on model)

b_e span of elevator (2.64 feet on model)

V   air velocity, feet per second

D   propeller diameter (2.04 feet on model)

n   revolutions per second

and

ρ mass density of air, slugs per cubic foot

α angle of attack of thrust line, degrees

i_t angle of stabilizer with respect to thrust line,
            degrees; positive when trailing edge is down

δ control-surface deflection, degrees

ϵ average downwash angle, degrees

β propeller blade angle at 0.75 radius (18° on
            model)

Side-force factor $\dfrac{10^5}{32} \displaystyle\int_{0.2}^{1.0} \dfrac{b}{D} \sin \beta \; d\!\left(\dfrac{r}{R}\right)$

c_w wing chord at any station

r   propeller radius to given section, feet

b   propeller blade width, feet

R   D/2, foot

l_t tail length

n_o tail-off aerodynamic center location, percent
            mean aerodynamic chord

n_p neutral-point location, percent mean aerodynamic
            chord

c_t tail chord at any station

$\dfrac{dC_m}{di_t}$ rate of change of pitching-moment coefficient with stabilizer setting

$\dfrac{dC_m}{dC_L}$ rate of change of pitching-moment coefficient with model lift coefficient

$\dfrac{d\epsilon}{d\alpha}$ rate of change of average downwash angle with angle of attack of thrust line

$\left(\dfrac{dC_L}{d\alpha}\right)_1$ rate of change of trim lift coefficient with angle of attack of thrust line

C_{m_t} pitching-moment coefficient required of tail for trim at elevator-fixed neutral-point location

$\dfrac{q_t}{q}$ ratio of effective dynamic pressure over the horizontal tail to free-stream dynamic pressure

$\dfrac{d(q_t/q)}{dC_L}$ rate of change of q_t/q with model lift coefficient

Subscripts:

o   tail off

e   elevator

r   rudder

f   flap

t_i isolated horizontal tail

t   horizontal tail; tab (when used with δ)

MODEL AND APPARATUS

The XBTK-1 airplane is a single-engine, single-place, carrier-based dive and torpedo bomber with a

full cantilever low wing. It has partial-span extensible slotted flaps, "picket-fence" dive brakes, adjustable stabilizer, and a fully retractable conventional landing gear. The elevator is aerodynamically balanced by a shielded horn type of balance (medium nose shape) in combination with a spring tab. Trim changes are accomplished with the adjustable stabilizer. At design gross weight the airplane carries a radar unit under the right wing panel and an auxiliary droppable fuel tank under the left wing panel in addition to one 1000-pound bomb under the fuselage. The physical characteristics of the airplane which were supplied by the manufacturer are presented in tables I, II, and III.

The model was supplied by the Fleetwings Division of the Kaiser Cargo Corporation. It was not checked for accuracy. A three-view drawing of the model, as received, is shown in figure 1 and photographs of the original model are presented in figures 2(a) and 2(b).

The center wing panel has an NACA 2416 airfoil section with no taper or twist and is set at 2° with respect to the thrust line. The outer panels have a 0.50 taper ratio and -2.2° geometric twist. The theoretical tip section is an NACA 4412. All of the tests reported herein were made with a wing dihedral of $8\frac{1}{4}^{\circ}$ in the outboard panel. The flaps are of the extensible slotted type constructed in three sections, namely, a center section below the fuselage of about 5.4 inches span on the model and two outboard sections which extend from the center section to the wing outer panels. For normal operation (all tests reported in this paper) these three sections operate as a single unit but when a torpedo is carried, the center-section flap is locked in the retracted position. Details of the flap positions for various deflections tested are presented in figure 3.

The model was normally tested with a radar dome under the right wing and a fuel tank under the left wing. Two 1/4-inch diameter dowels 1 inch long were placed in the leading edge of the wing 18.09 inches from the center line of the model to represent cannon.

The horizontal tail had a modified NACA 66,2-015 root section tapering to a modified NACA 66,2-009 theoretical tip section. The airfoils were modified

in that the cusped trailing edge was replaced by a
straight-line fairing which was tangent to the true
contour at the $0.70c_t$ station and extended to the
trailing edge. The elevator, which was statically
mass-balanced, had an area of about 28.2 percent of
the horizontal-tail area, was of constant percent
chord $\left(\frac{c_e}{c_t} = 0.30\right)$ up to the horn and was unsealed
for most of the tests. Details of the horizontal tail
surface and elevator are shown in figure 4.

The model configurations referred to in the text
and on the figures are as follows:

    1. <u>Cruising configuration:</u>
        <u>Flaps neutral</u>
        Landing gear retracted

    2. <u>Landing configuration:</u>
        <u>Flaps extended</u> (45°)
        Landing gear extended
            (a) Main wheels down
            (b) Wheel-well cut-out in wing open
            (c) Tail wheel down
            (d) Tail-wheel door open
            (e) Arresting hook extended

The precision of setting the angular deflections
of the movable surfaces on the model is estimated to be
as follows: i_t $\pm0^\circ5'$, δ_e $\pm0^\circ30'$, δ_f and δ_t $\pm1^\circ0'$.

Power was obtained from a 56-horsepower, three-
phase induction motor. The speed of this motor was
determined by observation of a cathode-ray oscillograph
which indicates the output of a small alternator con-
nected to the shaft of the motor. The time base for the
oscillograph pattern is controlled by an audio-oscillator of
the electrically driven tuning-fork type, the frequency
of which is known within 0.1 percent.

<center>TESTS</center>

<u>Test conditions.</u>- Tests of the complete model were
made at dynamic pressures of 9.21 and 16.37 pounds per
square foot, which correspond to airspeeds of about
60 and 80 miles per hour. The test Reynolds numbers

were about 685,000 and 910,000 based on the wing mean
aerodynamic chord of 1.22 feet. Because of the turbulence
factor of 1.6 for the Langley 7- by 10-foot tunnel,
effective Reynolds numbers (for maximum lift coefficients)
were about 1,000,000 and 1,460,000, respectively.

The tests of the isolated horizontal tail were made
at a dynamic pressure of 13 pounds per square foot,
corresponding to an airspeed of 71 miles per hour under
standard sea-level atmospheric conditions. The test
Reynolds number was about 323,000 based on the average
chord of 5.81 inches. The turbulence factor is 1.93
for the Langley 4- by 6-foot tunnel, and hence, the
the effective Reynolds number (for maximum lift coef-
ficient) was about 624,000 for these tests.

Test procedure.- The thrust calibration of the
model propeller was obtained by measuring the resultant
drag of the model (cruising configuration) for a range
of propeller speeds near zero lift. The thrust coeffi-
cients were then computed from the equation

$$T_c' = c_D - c_{D_R}$$

where c_D is the drag of the model with the propeller
removed. The torque coefficients were obtained from a
motor calibration (torque as a function of minimum
current) using the values of minimum current at each
propeller speed. The results of the propeller calibration
are presented in figure 5.

Using the data of figure 5, it is only necessary to
vary the propeller speed for a particular tunnel speed
to obtain a range of thrust coefficients assuming that
in the normal angle-of-attack range the propeller thrust
is independent of the angle of inclination of the pro-
peller at constant nD/V.

The effective thrust coefficients at which the
power-on tests were made are shown in figure 6 as a
function of lift coefficient for constant power with a
constant-speed propeller. These curves were supplied
by the manufacturer.

All tests were made at a dynamic pressure of
16.37 pounds per square foot except tests simulating

the take-off power condition in the landing configuration which were made at a dynamic pressure of 9.21 pounds per square foot. This difference was necessitated because of power limitations of the model motor.

The thrust coefficient at which windmilling tests were made was about -0.010.

CORRECTIONS

Langley 7- by 10-foot tunnel.- All data have been corrected for tares caused by the model support strut. Jet-boundary corrections have been applied to the angles of attack, the drag coefficients, and the tail-on pitching-moment coefficients. The corrections were computed as follows:

$$\Delta\alpha = 57.3 \; \delta_w \; \frac{S}{C} \; C_L \; \text{(degrees)}$$

$$\Delta C_D = \delta_w \; \frac{S}{C} \; C_L^2$$

$$\Delta C_m = -57.3\left(\frac{\delta_T}{\sqrt{q_t/q}} - \delta_w\right) \frac{S}{C} \frac{dC_m}{di_t} C_L$$

where

δ_w jet-boundary correction factor at the wing (0.116)

δ_T total jet-boundary correction factor at the tail (0.196)

S   model wing area (8.55 square feet)

C   tunnel cross-sectional area (69.59 square feet)

$\dfrac{dC_m}{di_t}$ rate of change of pitching-moment coefficient with stabilizer setting as determined in tests

$\dfrac{q_t}{q}$ ratio of effective dynamic pressure over the horizontal tail to free-stream dynamic pressure

All jet-boundary corrections were added to the test data.

Langley 4- by 6-foot tunnel.- The angles of attack of the tail have been corrected for the effect of the jet boundaries. The correction was added to the measured values and was as follows:

$$\Delta\alpha_t = 1.097C_{L_t} \text{ (degrees)}$$

The lift coefficients were corrected for support-strut tares. No tares or jet-boundary corrections were applied to the hinge-moment coefficients inasmuch as these corrections were estimated to be negligible.

PRESENTATION OF DATA

Tests were made at various stabilizer settings for several power and model conditions. These tests were made with the elevator both fixed at 0° and free to float. Elevator and elevator-tab tests were also made on the complete model for similar power and model conditions. In addition, isolated horizontal-tail characteristics were determined. Several slotted flap deflections were tested. Photographs of tufts placed on the wing were made to determine the stall progression for several power and model conditions.

A short outline of the figures showing the results of the longitudinal stability and control investigation is presented in the following table:

DISCUSSION

Elevator-fixed stability.- The elevator of the
XBTK-1 airplane is equipped with a spring tab. With
the stick fixed, the elevator, therefore, is not
necessarily fixed as is true for a conventional control
system without cable stretch. However, neutral points
obtained from flight data are generally determined from
the variation of elevator angle with velocity rather
than the variation of stick position with velocity. Thus,
the presence of the spring may be treated as an additional
source of flexibility in the control system and neutral
points can then be obtained by usual methods. (See refer-
ence 1.)

The static margin is positive for all conditions
tested at all contemplated airplane center-of-gravity
locations. (See fig. 8.) The effect of power on the
longitudinal stability was unusually small.

The propeller used on the model was of the same
diameter as the scaled-down airplane propeller diameter
but the side-force factor was 65.8 as compared to an

airplane value of 91.3. However, a similar difference of
model and airplane propeller side-force factors in
another investigation was found to give a forward
neutral-point shift of less than 0.01 mean aerodynamic
chord. Inasmuch as this value is well within the
accuracy of the neutral-point calculation, it can be
neglected.

An attempt has been made to analyze the effects
of power on the longitudinal stability. In order to do
this various factors which affect the stability of the
airplane have been calculated and are shown on figure 9.
It may be shown that for neutral stability and assuming
a constant tail lift-curve slope

$$\frac{dC_m}{dC_L} = 0$$

$$= \left(\frac{dC_m}{dC_L}\right)_o - \frac{\frac{S_t l_t}{Sc}\left(\frac{\delta C_L}{\delta \alpha}\right)_{t_1} \frac{q_t}{q}\left(1 - \frac{d\epsilon}{d\alpha}\right)}{\left(\frac{dC_L}{d\alpha}\right)_1} + \frac{C_{m_t}}{\frac{q_t}{q}}\frac{d\left(\frac{q_t}{q}\right)}{dC_L} \qquad (1)$$

which reduces to

$$n_p = n_o + \frac{\left|\frac{dC_m}{di_t}\right|}{\left(\frac{dC_L}{d\alpha}\right)_1}\left(1 - \frac{d\epsilon}{d\alpha}\right) - \frac{C_{m_t}}{\frac{q_t}{q}}\frac{d\left(\frac{q_t}{q}\right)}{dC_L} \qquad (2)$$

inasmuch as

$$\left|\frac{dC_m}{di_t}\right| = \frac{S_t l_t}{Sc}\left(\frac{\delta C_L}{\delta \alpha}\right)_{t_1} \frac{q_t}{q}$$

and

$$n_p - n_o = \left(\frac{dC_m}{dC_L}\right)_o \text{ (at the neutral point)}$$

where the notations are as previously defined in the
text.

Thus, the relative weight of the various factors which contribute both favorably and unfavorably to the longitudinal stability can be estimated for any condition from the preceding equations. In addition, the effects of power can be separated to some degree.

In the cruising configuration and at moderate lift coefficients the model has more stability with take-off power than it does with the propeller windmilling. Using figures 7 and 9 to obtain the values of the various stability determinants at $C_L = 0.8$, it is found from equation (2) that the stabilizing effects of a rearward movement of n_o (0.055 mean aerodynamic chord) and of increased $\frac{d(q_t/q)}{dC_L}$ at the tail (0.030 mean aerodynamic chord) more than compensate for the 0.060 mean aerodynamic chord loss in stability caused mainly by a higher value of $\partial\epsilon/\partial\alpha$ with power. Thus, the total change in stability due to power at $C_L = 0.8$ as determined from the summation of individual effects is found to be a 0.025 mean aerodynamic chord rearward shift of the neutral point. This value compares with the measured value of 0.022 mean aerodynamic chord (fig. 8). The discrepancy is quite small in this instance and, in general, it is believed to be within the accuracy of the neutral-point determination (approximately 0.02 mean aerodynamic chord).

At very low-lift coefficients the stability in the cruising configuration becomes less power on than power off. This is seen to be chiefly caused by the rate of change of dynamic pressure at the tail. For while at a higher coefficient $\frac{d(q_t/q)}{dC_L}$ is responsible for a favorable effect, $\Delta n_p = 0.03$ mean aerodynamic chord, at $C_L = 0.2$ an adverse shift of $\Delta n_p = 0.015$ is realized. The main reason for this change is that the tail load for trim is negative and hence favorable at higher lift coefficients but becomes positive at low values of C_L.

In the landing configuration the change in neutral-point location with the application of power is fairly constant, small, and always stabilizing. (See fig. 8.) This may be explained by the extremely

large rearward shift in tail-off aerodynamic center
location with power. The difference in n_o increases
at high lifts and thus counteracts the loss in the
stability contributed by the empennage, inasmuch as
progressively larger values of $d\epsilon/d\alpha$ and
$\dfrac{d(q_t/q)}{dC_L}$ are both destabilizing.

Some of the design features, which may in part
account for the small change in stability with power
through the lift range as well as the over-all satis-
factory stability characteristics, are the high loca-
tion of the horizontal tail and rectangular inboard
wing panels with constant chord flaps. Data showing
favorable effects of the two aforementioned model
features can be found in reference 2. In addition, the
design center-of-gravity location is considerably below
the thrust line so that the direct thrust moment is
favorable.

. Elevator-free stability.- The static margin will be
positive for all conditions tested at all contemplated
airplane center-of-gravity locations with the elevator
free (fig. 11).

In general, the elevator-free neutral points are
from 0 to 6 percent mean aerodynamic chord farther aft
than the corresponding elevator-fixed neutral points for
similar conditions. Compare figures 11 and 8. An
exception to this trend is found in the take-off power
condition, in the landing configuration, and at high
lift coefficients where the stability is considerably
less with the elevator free.

It can be seen from the isolated-tail data of
figure 12 that the ratio of the hinge-moment parameters
$-\dfrac{\left(\partial C_{h_e}/\partial\alpha\right)_{t_1}}{\left(\partial C_{h_e}/\partial\delta\right)_{t_1}}$ which determines the floating characteristics
of the elevator is of such sign as to cause the elevator
to float against the relative wind and thus increase
the tail effectiveness and hence the stability (inasmuch
as $d\epsilon/d\alpha$ is less than unity). Apparently, however, in
the landing configuration with take-off power $\left(dC_{h_e}/d\alpha\right)_t$
becomes negative at high-lift coefficients (fig. 14(e))
thus reducing the tail effectiveness. It might be noted

that this change in $\left(dC_{h_e}/d\alpha\right)_t$ is probably a result
of the nonlinear hinge-moment characteristics (fig. 12)
combined with a large reduction in tail angle of attack
over the right inboard portion of the tail and a similar
increase in angle of attack over the left inboard portion
which is caused by right-hand propeller operation (refer-
ence 3). The greatest part of the decrease in stability
is not thought to be caused by a reduction in tail
effectiveness due to negative $\left(dC_{h_e}/d\alpha\right)_t$ but rather
by the rate of change of tail effectiveness with lift
coefficient. Thus, in order to determine the power
effects with the elevator free, the following term must
be added to equation (2):

$$\frac{-C_{m_t}}{\left(\dfrac{dC_L}{d\alpha}\right)_t}\; \frac{d\left(\dfrac{dC_L}{d\alpha}\right)_t}{dC_L}$$

where the notation used has been previously defined.

The elevator-free curves shown as dashed lines on
figures 10(a) and 10(b) were obtained by cross-plotting
the hinge-moment data of figures 14(a) and 14(b). This
was necessary inasmuch as severe oscillations of the
elevator occurred with the stabilizer incidence set at
a value lower than 3° or 4° in the cruising configura-
tion. This might be attributed to a positive value
of $\left(dC_{h_e}/d\alpha\right)_t$.

The presence and type of oscillations on the air-
plane will depend on such factors as control surface
and airplane inertia, control system friction, stability,
and certain other factors. (See reference 4.)

Isolated horizontal tail.- A series of tests was
made for various elevator and elevator-tab settings on
the isolated horizontal tail. (See figs. 12 and 13.)
The elevator-free curve, shown on figure 12, was obtained
using the hinge-moment data. The difference between the
hinge-moment curves at zero tab and elevator deflections
(figs. 12 and 13) may be attributed to the fact that these
tests were run at different times and the differences in
the two curves are an indication of the experimental
accuracy.

The following table summarizes the elevator parameters:

	Original	Gap sealed	Elevator free
$\left(\dfrac{\partial C_L}{\partial \alpha}\right)_{t_1}$	0.0565	0.0575	0.069
$\left(\dfrac{\partial C_L}{\partial \delta}\right)_{t_1}$	.034	------	------
$\left(\dfrac{\partial C_{h_e}}{\partial \alpha}\right)_{t_1}$	= 0.000 (average for two tests)	------	------
$\left(\dfrac{\partial C_{h_e}}{\partial \delta}\right)_{t_1}$	-0.0057	------	------

As is shown by the preceding table, sealing the gap increased the lift-curve slope by about 2 percent, which is of the expected magnitude inasmuch as the gap was only from about 0.001 to $0.002c_t$.

The slope of the elevator-free lift curve showed about a 22-percent average increase over the elevator-fixed slope. Although this appears contradictory in view of the tabulated value of $\left(\partial C_{h_e}/\partial \alpha\right)_{t_1}$, it must be remembered that the hinge-moment characteristics are nonlinear and the tabulated value is an average value of slopes measured over a small angle-of-attack range at the origin.

The tab effectiveness $\left(\partial C_{h_e}/\partial \delta_t\right)_{t_1}$ averaged about -0.0053 at moderate deflections in the angle-of-attack range likely to be encountered under normal operating conditions of the airplane.

Effect of elevator and elevator-tab deflection.- The elevator effectiveness as determined from figure 14(a) is about 0.9 as high as that obtained from isolated-tail data using the relationship

$$\frac{\partial C_m}{\partial \delta_e} = -\left(\frac{\partial C_L}{\partial \delta_e}\right)_{t_1} \times \frac{S_t l_t}{S q} \qquad (3)$$

where the symbols have been previously denoted in the text. This effectiveness ratio of 0.9 indicates that the average dynamic pressure over the elevator on the complete model is about 0.9 of the free stream q.

The data (fig. 14) indicate that the elevator should be sufficiently powerful to trim the airplane at any speed away from the ground for all conditions.

As has been stated earlier in the text, a large degree of the aerodynamic balance of the elevator is supplied by a spring tab. Although it is beyond the scope of this paper to present detailed control-force characteristics, estimates using the hinge-moment data of figures 14 and 15 indicate that the control forces for conditions of steady flight will be very light if the spring stiffness contemplated for the prototype airplane is used. However, since it is believed to be a relatively simple task to change the spring constant on the airplane, no major difficulty is likely to be encountered in obtaining a spring constant which will give satisfactory stick-force characteristics.

The power-off tab effectiveness $dC_{h_e}/d\delta_t$ (figs. 15 (a) and 15(c)) agrees well with that obtained from isolated-tail tests. It might be noted that the ratio of $\dfrac{dC_{h_e}}{d\delta_t} \Big/ \dfrac{dC_{h_e}}{d\delta_e}$ increases with C_L for the power-on conditions, indicating that the average dynamic pressure over the tab is greater than that over the elevator. This increases the spring-tab effectiveness but has no bearing on elevator-free stability inasmuch as the tab is not used for trimming purposes.

It may also be noted from the data of figure 15 that tab deflection appears to have a considerable effect on the pitching-moment curve. It is believed, however, that the neutral-point location will be negligibly affected by tab deflection because of the small spring-tab deflections which will be required with trim elevator deflections at the center of gravity for neutral stability.

Effect of slotted-flap deflection.- Tail-off data
were obtained at various slotted-flap deflections.
(See fig. 16.) The maximum lift coefficients obtained
from this figure are tabulated in the following table
and have been corrected for tail load required for trim
at the design center-of-gravity location.

Configuration	δ_f (deg)	$C_{L_{max}}$
Cruising	0	1.34
Landing	30	1.79
	35	1.78
	40	1.84
	45	1.84

The change in maximum lift coefficient when the
flap deflection is increased from 30° to 45° is seen
to be quite small. It may also be seen that at angles
of attack slightly below the stall an appreciable
increment in lift is obtained when the flap deflection
is increased in the higher range.

Stalling characteristics.- Photographs of the tufts
showing the stall progression are shown for the different
model configurations. (See figs. 17 through 22.)

In the windmilling, cruising configuration, the
stall appears to start at the trailing edge slightly
inboard of the fold line. As the angle of attack is
increased the stall progresses forward over the inboard
wing panel while not progressing markedly toward the
tip. The final photograph (fig. 17) at $\alpha = 17.3°$
shows the inboard wing panels almost completely stalled
while over a large portion of the outboard panel the
flow is merely unsteady. Removal of the radar, wing
tank, and guns seems to have a very slight effect on
the stall progression in the cruising configuration.
(Compare figs. 17 and 18.) When take-off power is
applied in the cruising condition, the portion of the
wing immersed in the slipstream remains unstalled after
most of the remainder of the wing is stalled. The stall
appears to be earlier and more pronounced over the left
inboard wing panel than it is over the right panel which
might be expected for right-hand propeller operation
(fig. 19).

In·the landing condition, with the propeller wind-
milling, the flaps appear to be generally stalled or in
a region of unsteady flow at low angles of attack. As
the angle of attack increases, the flow through the slot
improves and the flaps become unstalled. The wing
remains unstalled up to about 15° or 16° angle of attack.
The stall then begins at the left inboard fold line.
spreading inboard much more rapidly than it progresses
toward the tip. The last photograph on figure 20 shows
that while a good portion of the left panel is stalled,
the right panel is either unstalled or only in a region
of unsteady flow at α = 18.1°, except at the extreme
right wing tip where stall has begun. The pictures on
figure 21, guns, radar, and fuel tank off would seem
to indicate that the absence of the latter auxiliary
equipment causes stall over the left inboard panel much
earlier than is shown in figure 20 (auxiliary equipment
on). The reason for this effect is not known. Otherwise,
except for a lesser tendency for tip stall on the right
wing tip, the progression of the stall with and without
the auxiliary equipment is similar. The chief effect
of power on the stall is again a stall delay in regions
close to the wing-fuselage juncture (fig. 22).

Because of differences in scale, the amount of stall
indicated at each angle may differ from that on the
full-scale airplane but the stall progression should be
correct.

CONCLUSIONS

The results of the longitudinal stability and control
investigation of a 0.15-scale model of the XBTK-1 air-
plane indicate that:

1. The longitudinal stability will probably be
satisfactory for all probable flight conditions at the
rearmost center-of-gravity location with the elevator
both fixed and free. Power effects were quite small.

2. Sufficient elevator control will be available
to trim in any flight condition away from the ground.
Indications are that the stick forces may be light if
the spring stiffness now contemplated is used.

3. Increasing the slotted flap deflection above 30°
increased $C_{L_{max}}$ only slightly.

4. Stalling characteristics will probably be
satisfactory. In general, stall started at the wing
fold line and spread inboard faster than toward the tip.
Power delayed stall over portions of the wing immersed
in the slipstream. The presence of the fuel tank, radar,
and wing guns do not appreciably affect the stall trends.

Langley Memorial Aeronautical Laboratory
    National Advisory Committee for Aeronautics
        Langley Field, Va.

REFERENCES

1. Schuldenfrei, Marvin: Some Notes on the Determination
      of the Stick-Fixed Neutral Point from Wind-Tunnel
      Data. NACA RB No. 3I20, 1943.

2. Weil, Joseph, and Wells, Evalyn G.: Wind-Tunnel Tests
      of the 1/8-Scale Powered Model of the Curtiss XBTC-2
      Airplane. I - Preliminary Investigation of Longi-
      tudinal Stability. NACA MR, June 1, 1944.

3. Pass, H. R.: Wind-Tunnel Study of the Effects of
      Propeller Operation and Flap Deflection on the
      Pitching Moments and Elevator Hinge Moments of a
      Single-Engine Pursuit-Type Airplane. NACA ARR,
      July 1942.

4. Greenberg, Harry, and Sternfield, Leonard: A Theoretical
      Investigation of Longitudinal Stability of Airplanes
      with Free Controls Including Effect of Friction in
      Control System. NACA Rep. No. 791, 1944.

TABLE I

DESCRIPTION OF FLEETWINGS XBTK-1 AIRPLANE

Name and type . . . . . XBTK-1 (Navy dive-torpedo bomber)
Engine . . . . Pratt & Whitney R-2800-22W
Ratings:

Normal power . . $\begin{cases} \text{1700 bhp at 2600 rpm at sea level} \\ \text{1700 bhp at 2600 rpm at 7000 ft} \\ \text{1450 bhp at 2600 rpm at 18,500 ft} \end{cases}$

Take-off power . . 2100 bhp at 2800 rpm at sea level

Military power . . $\begin{cases} \text{2100 bhp at 2800 rpm at 1000 ft} \\ \text{1600 bhp at 2800 rpm at 16,000 ft} \end{cases}$

Propeller . . . . Hamilton Standard
    Diameter, ft 13.58
    Blades (number and designation) . . . . . four, 2C15B1
    Gear ratio 0.45
    Activity factor 95.6
    Blade thickness $(h/b)_{0.75R}$ 0.060

Normal gross weight, lb 14,850
Over-all length, ft 39.0
Over-all height, ft 11.86
Wing span, ft 48.67

NATIONAL ADVISORY
COMMITTEE FOR AERONAUTICS

TABLE II

AIRPLANE WING- AND TAIL-SURFACE DATA

	Wing	Horizontal tail	Vertical tail
Area, sq ft	380	80	[a]51.25
Span, ft	48.67	18.5	8.38
Aspect ratio	6.23	4.26	1.42
Taper ratio	.50	.59	-------------
Dihedral, deg	8.25	0	-------------
Incidence, deg	2	2 to -7	0
Geometric twist, deg	-2.2	0	0
Root section	NACA 2416	NACA 66.2-015 modified	NACA 66.2-015 modified
Tip section	NACA 4412	NACA 66.2-009 modified	NACA 66.2-009 modified
Mean aerodynamic chord, ft	8.17	-------------	-------------
Root chord, ft	9.17	5.45	6.89
Theoretical tip chord, ft	4.585	3.20	2.67

[a]Includes dorsal fin.

NATIONAL ADVISORY
COMMITTEE FOR AERONAUTICS

TABLE III

AIRPLANE CONTROL-SURFACE DATA

	Ailerons	Elevators	Rudder	Flaps	Dive brakes
Percent span	54.0	95.0	100	43.1	Upper 31.4 Lower 35.1
Area, aft of hinge line, sq ft	36.86	22.50	15.66	42.0	------------
Balance area, sq ft	15.11	2.96	[a]5.02	-----	------------
Trim-tab area, sq ft	[b].52	None	1.00	-----	------------
Percent span	2.8	-----------	23.0	-----	------------
Tab travel, deg	±15	-----------	±5	-----	------------
Balance tab area, sq ft	2.76	3.36	1.00	-----	------------
Percent span	13.3	35.7	23.0	-----	------------
Tab travel, deg	±15(±30 lb)	±15(±55 lb)	±15($\delta_t = -0.518\delta_r$)	-----	------------
Control travel, deg	±15	15, -25	±30	45	[c]Upper 73 Lower 80
Root mean square chord, ft	1.37	1.27	1.90	2.06	Upper 1.45 Lower 1.55
Distance to hinge line from normal c.g. (25.6), ft	------------	22.00	23.67	-----	------------

[a]1.20-square-foot horn.
[b]Left aileron only.
[c]Measured from airfoil contour.

<u>Flap deflections (corresponding powers)</u>

Landing, deg . . . . . . 45 (power off)
Take-off, deg . . . . . 32.5 (2100 hp)
All other conditions . flaps retracted
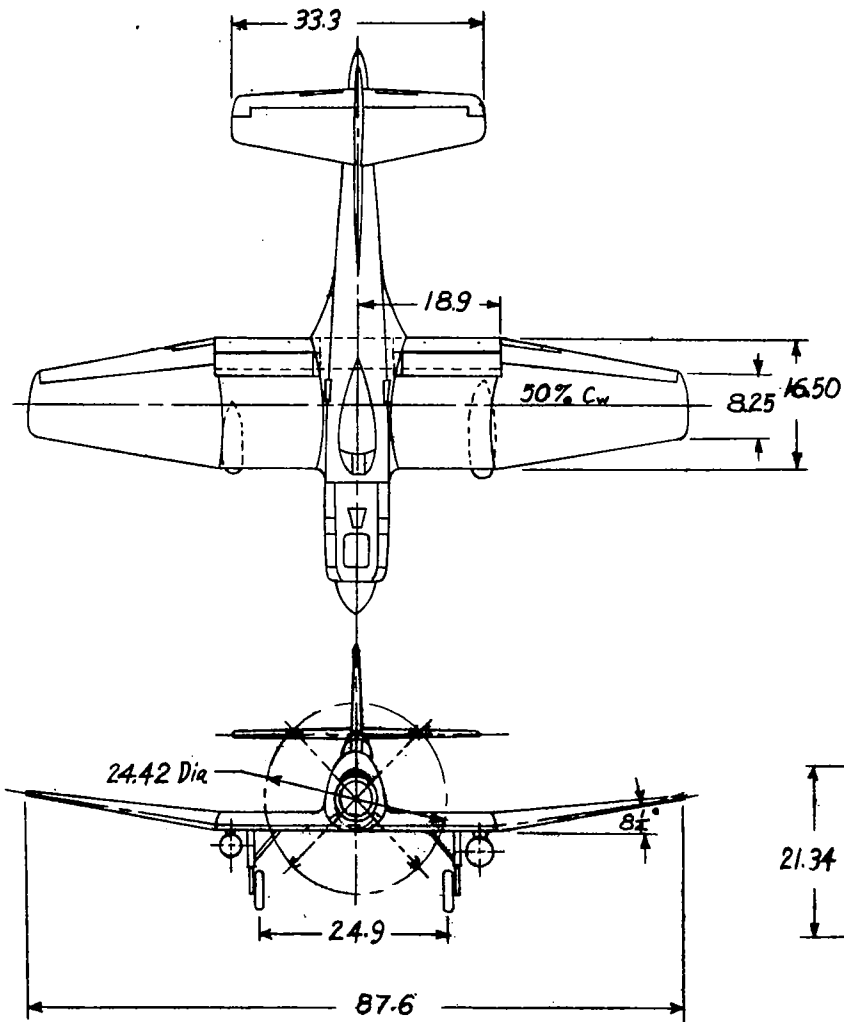
Root section – NACA 2416
Tip section – NACA 4412
Wing area – 8.55 ft.²
M.A.C. = 14.64 in.
Design CG (Wheels up) 25.6 % MAC
Taper ratio, outboard panel – .50
Geometric twist of outboard panel – -2.2°
Incidence of inboard panel – 2°0'.

All dimensions in inches

33.3

18.9

50% C_w

8.25   16.50

24.42 Dia

8¼°

24.9

87.6

70.20

design (wheels up) C.G.

₵ Thrust

21.34

39.60

12°
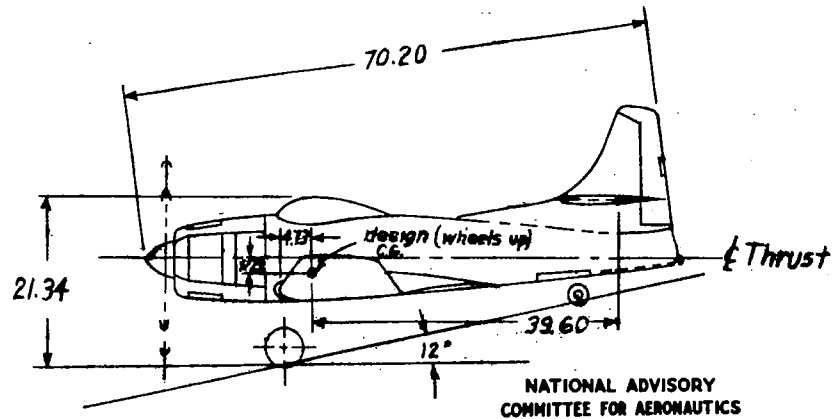
NATIONAL ADVISORY
COMMITTEE FOR AERONAUTICS

Figure 1 .– Three view drawing of 0.15-scale model of Fleetwings XBTK-1 airplane.
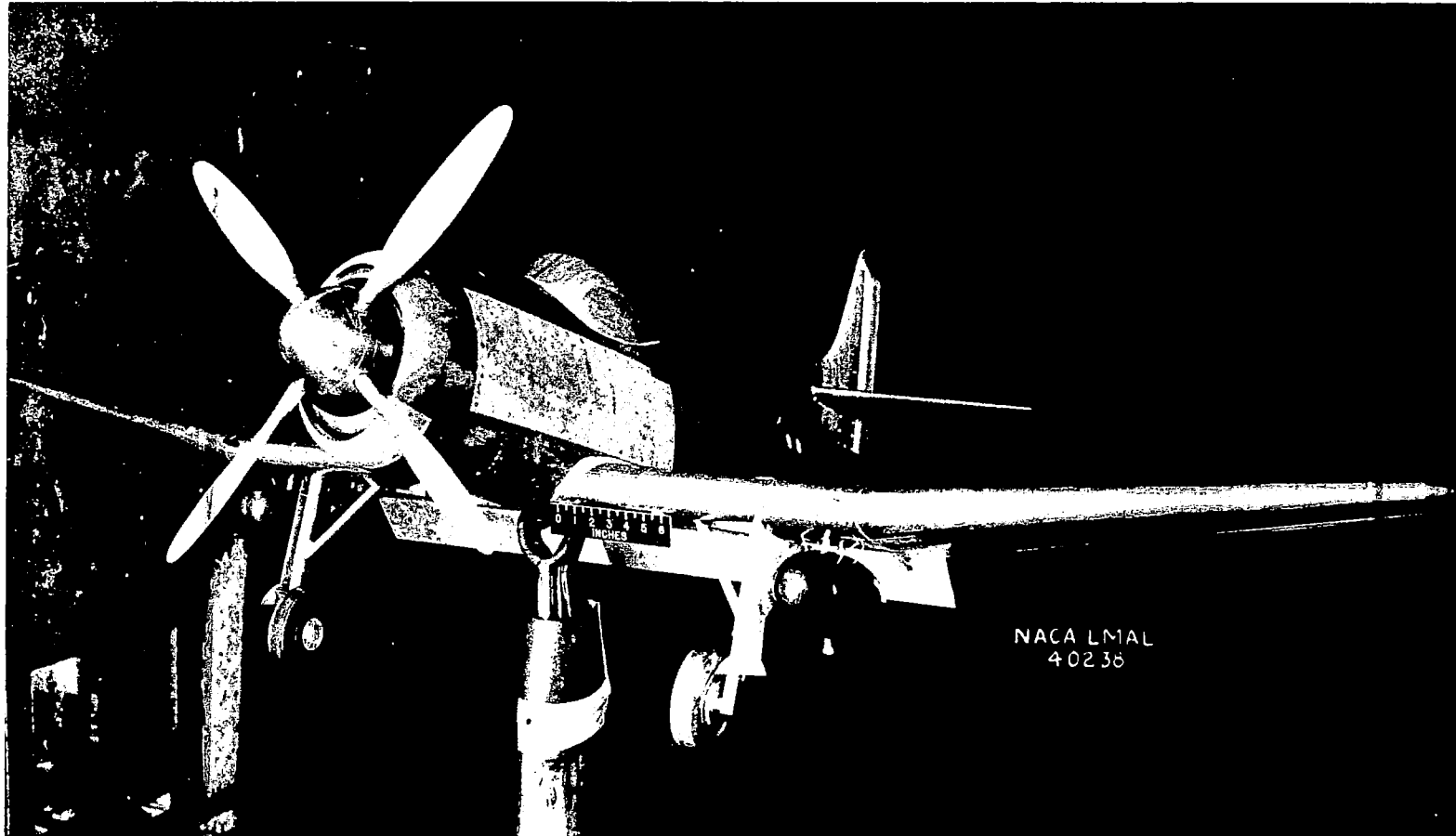
Figure 2(a).- Three-quarter front view of the 0.15-scale model of the
XBTK-1 airplane.
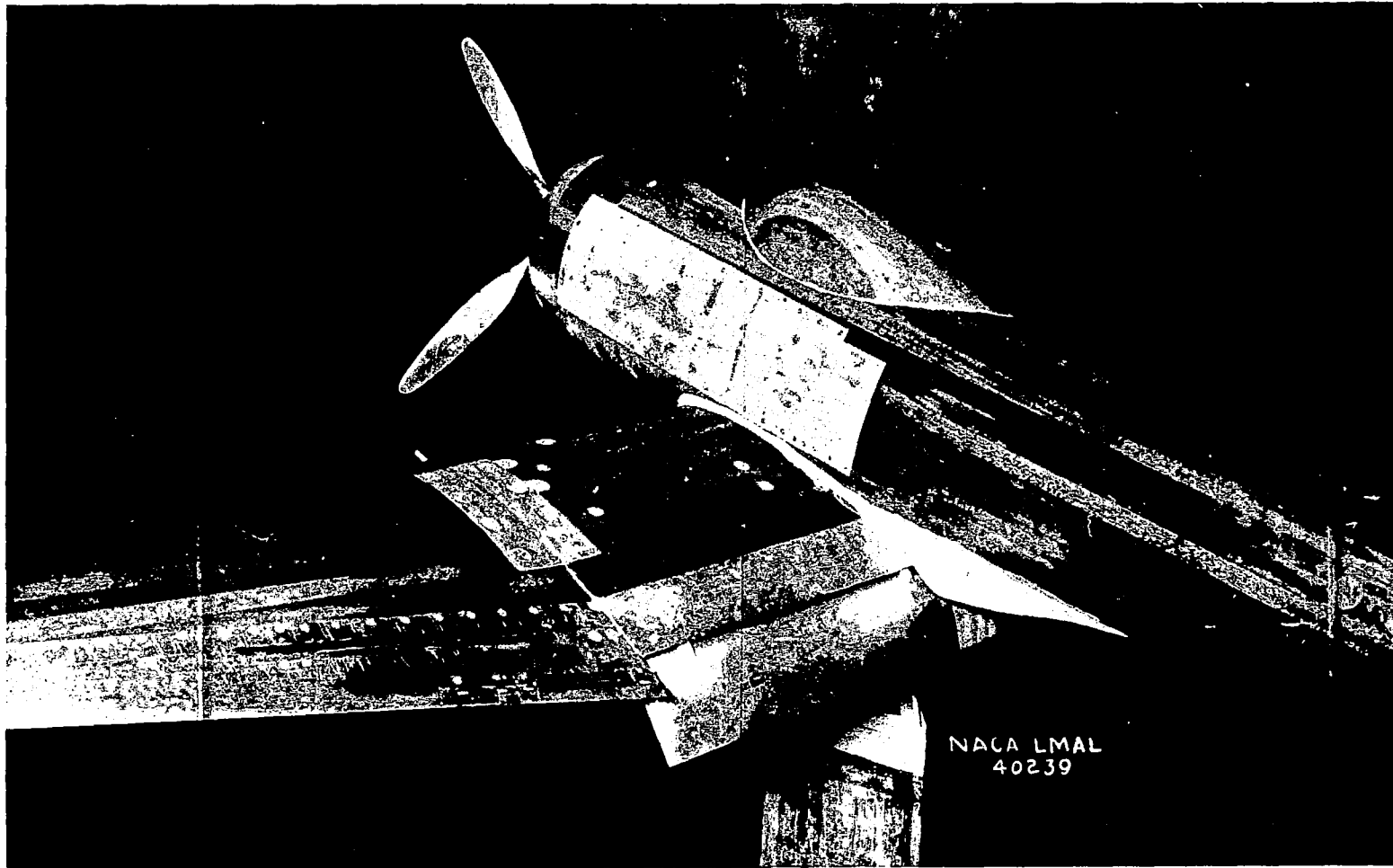
Figure 2(b).- Three-quarter rear view of the 0.15-scale model of the
X BTK-1 airplane.

.039c_w

.024c_w gap

Wing
chord line

c_f

30°

.033C_w

.024c_w gap

35°

.032C_w

.023c_w gap

40°

.027C_w

.022c_w gap

45°

$c_f/c_w = .225$
$c_w = 16.50$ in.
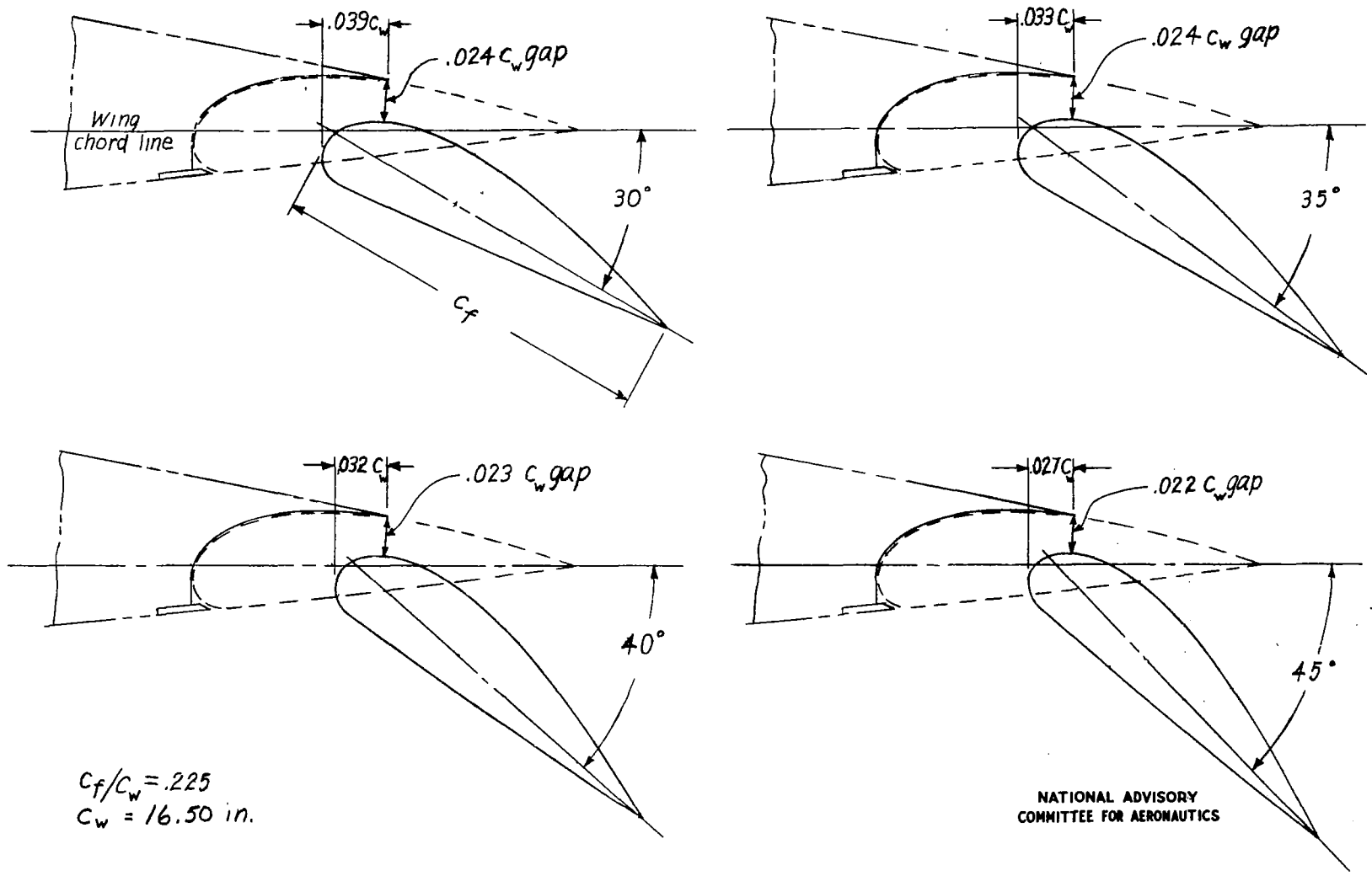
Figure 3 .- Details of slotted flap positions for various deflections tested on the 0.15 scale model of the XBTK-1 airplane.
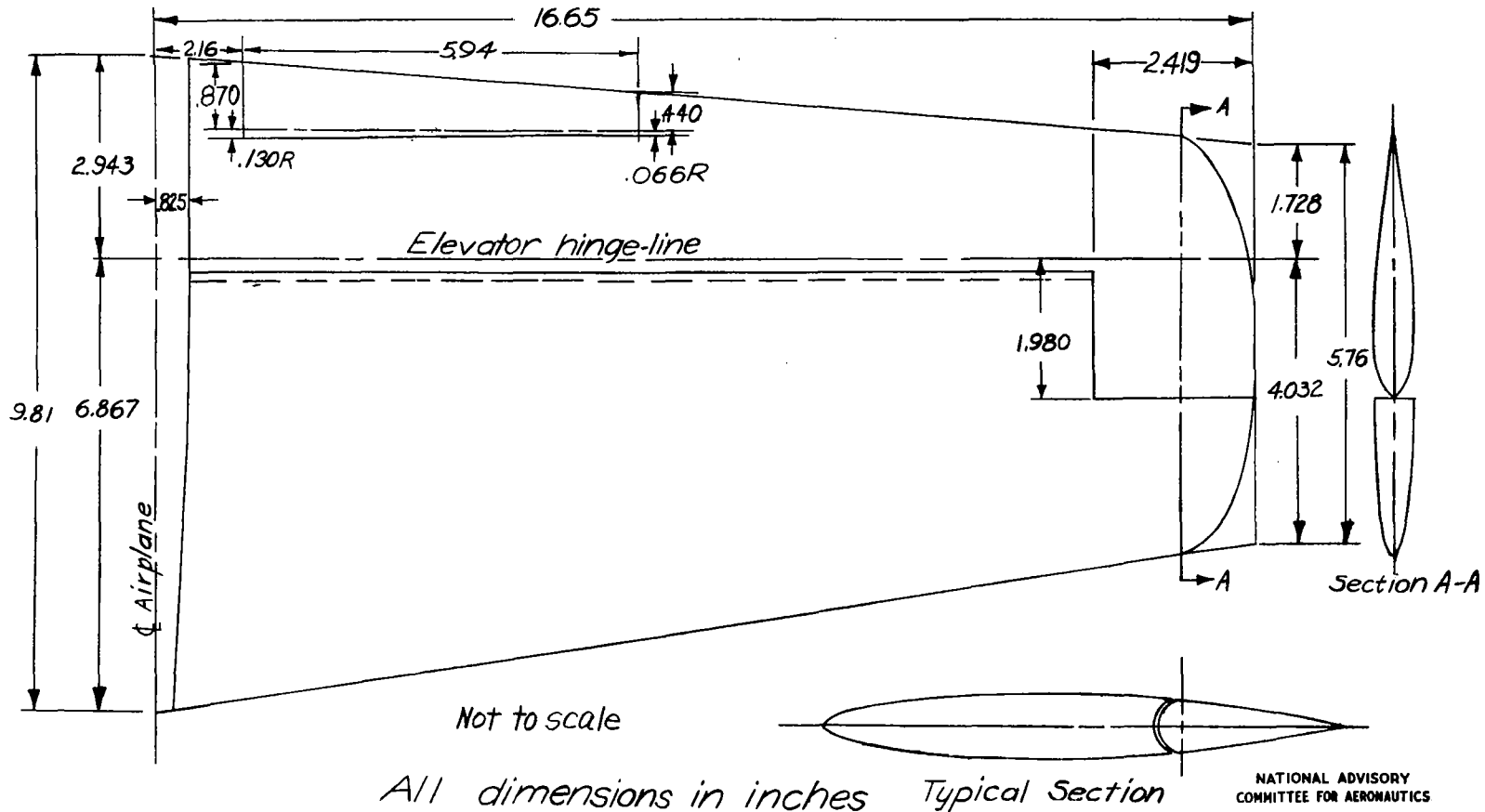
Figure 4.- Drawing of horizontal tail of 0.15-scale model of the XBTK-1 airplane

16.65

2.16

5.94

2.419

.870

.440

.130R

.066R

2.943

.825

Elevator hinge-line

1.728

A

1.980

5.76

9.81 6.867

4.032

¢ Airplane

A

Section A-A

Not to scale

All dimensions in inches

Typical Section

NATIONAL ADVISORY
COMMITTEE FOR AERONAUTICS

Figure 5 - Characteristics of a 2.04 ft. diameter four-bladed propeller on 0.15 scale model of XBTK-I airplane. $\alpha = 0°$, $\beta = 18°$
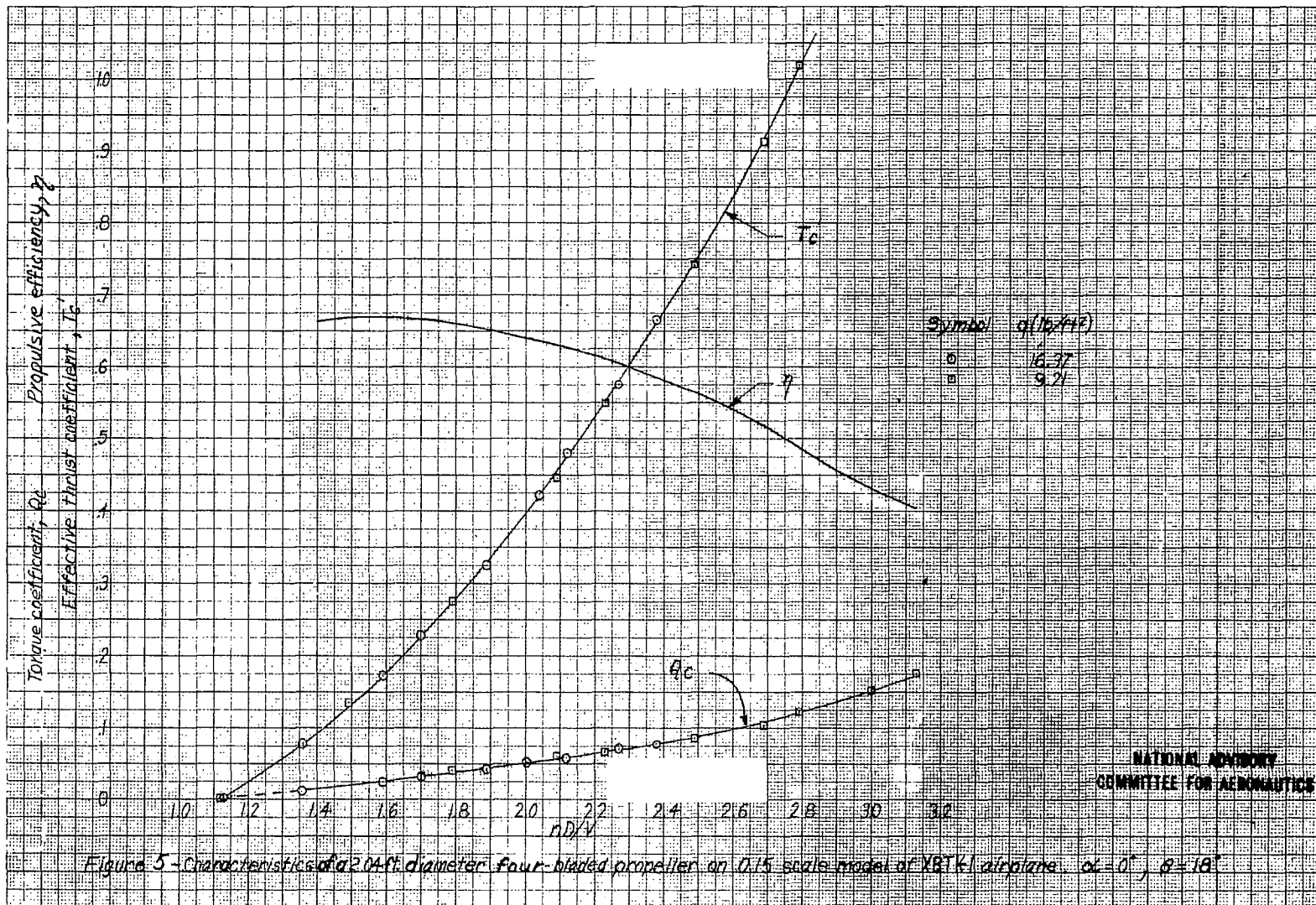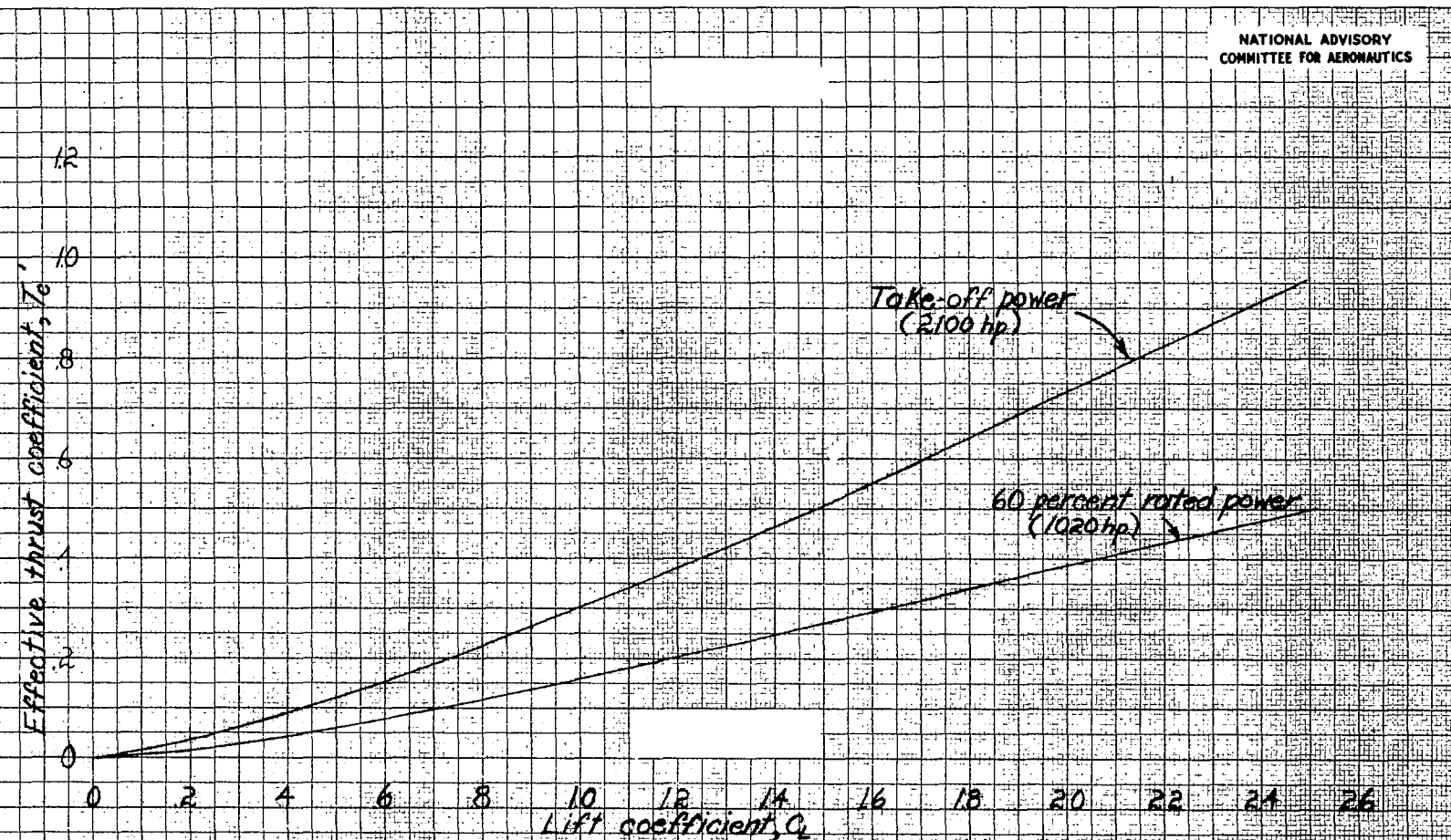
Figure 6.-Thrust coefficient available at any lift coefficient for the XBTK-1 airplane with 60 percent rated and take-off power. Sea level conditions, $w/s = 39.1$
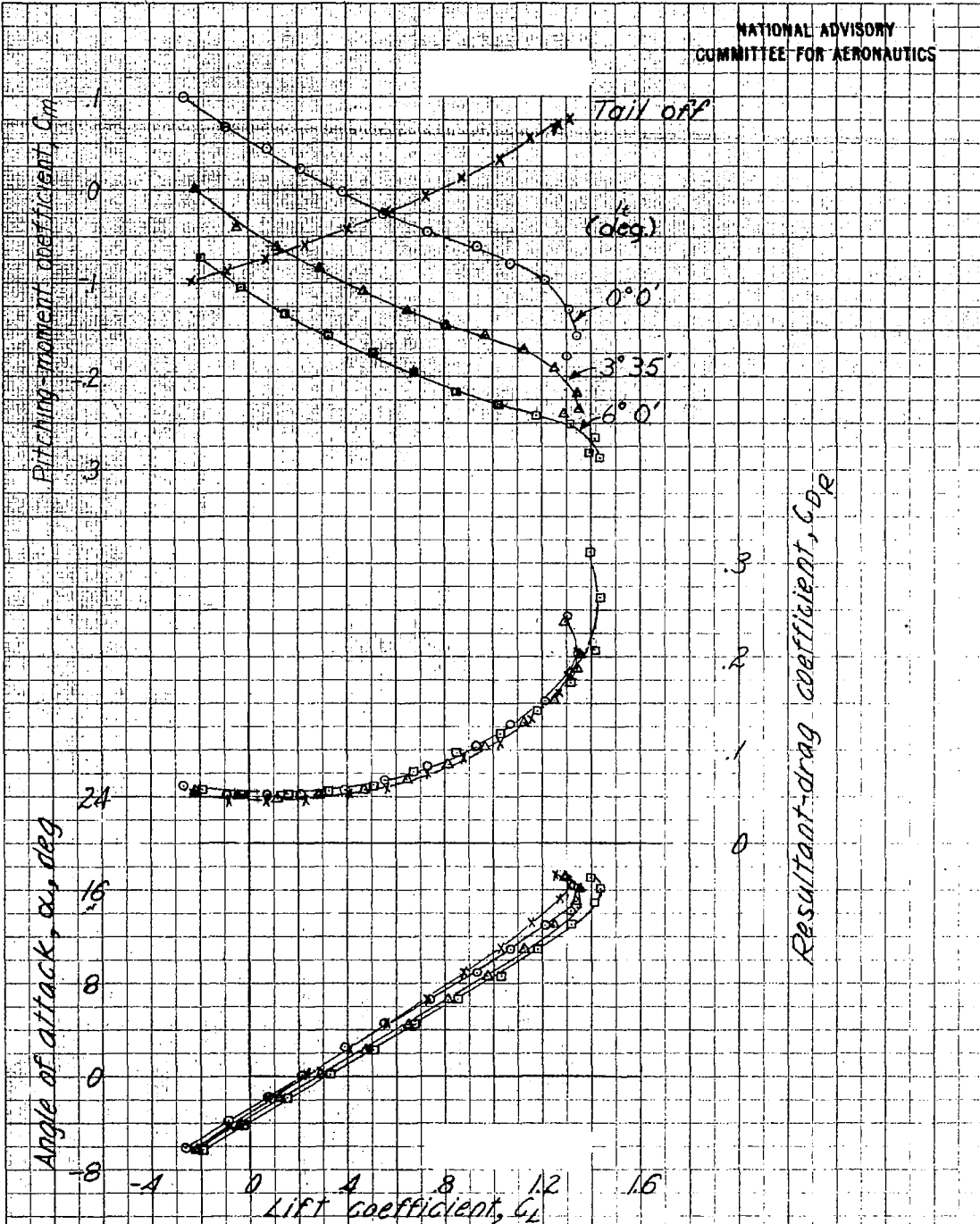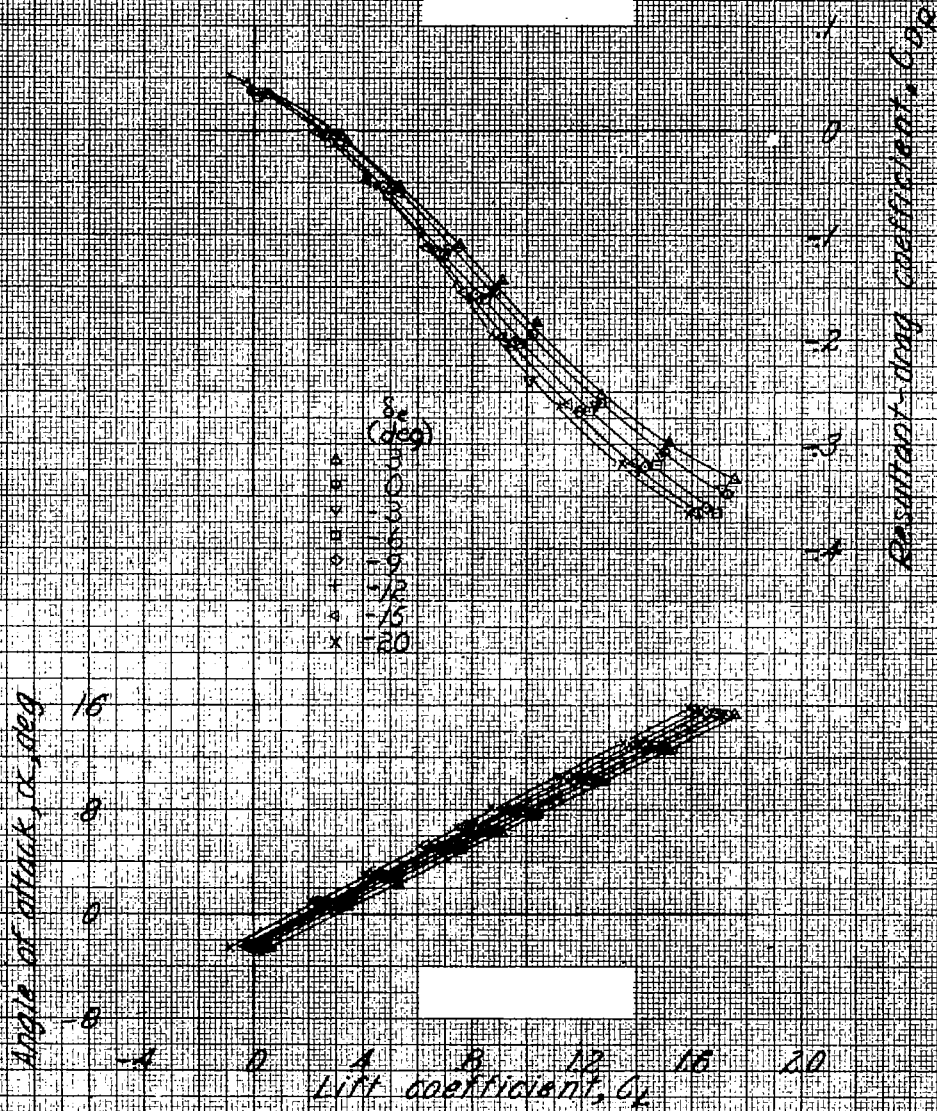
(a) Windmilling, cruising configuration

Figure 7 — Effect of stabilizer on the aerodynamic characteristics in pitch of the 0.15-scale model of the XBTK-1 airplane.
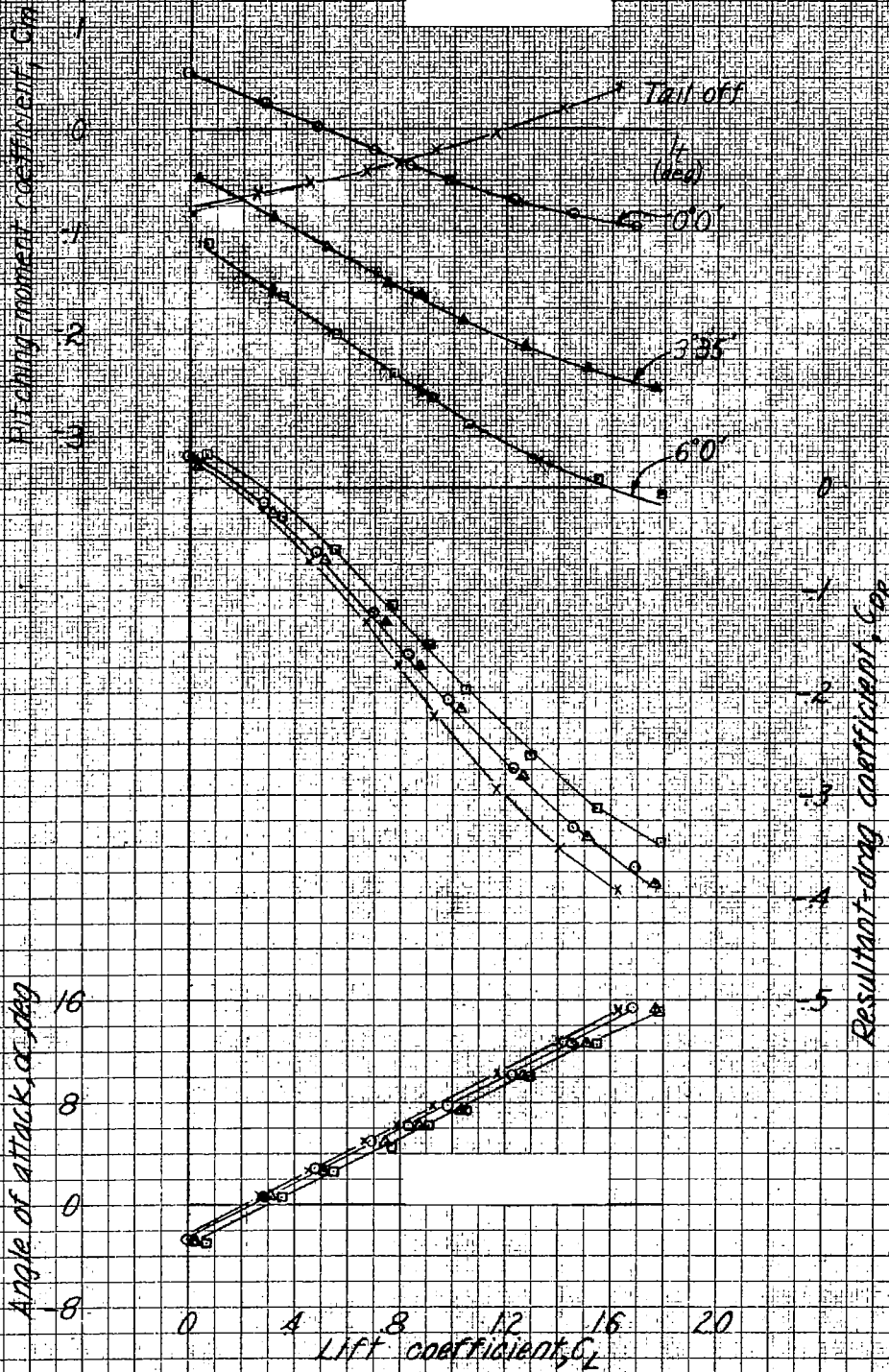
(b) Take-off power, cruising configuration

Figure 7.- continued

(c) Windmilling, landing configuration

Figure 7.- continued

(d) Take-off power, landing configuration
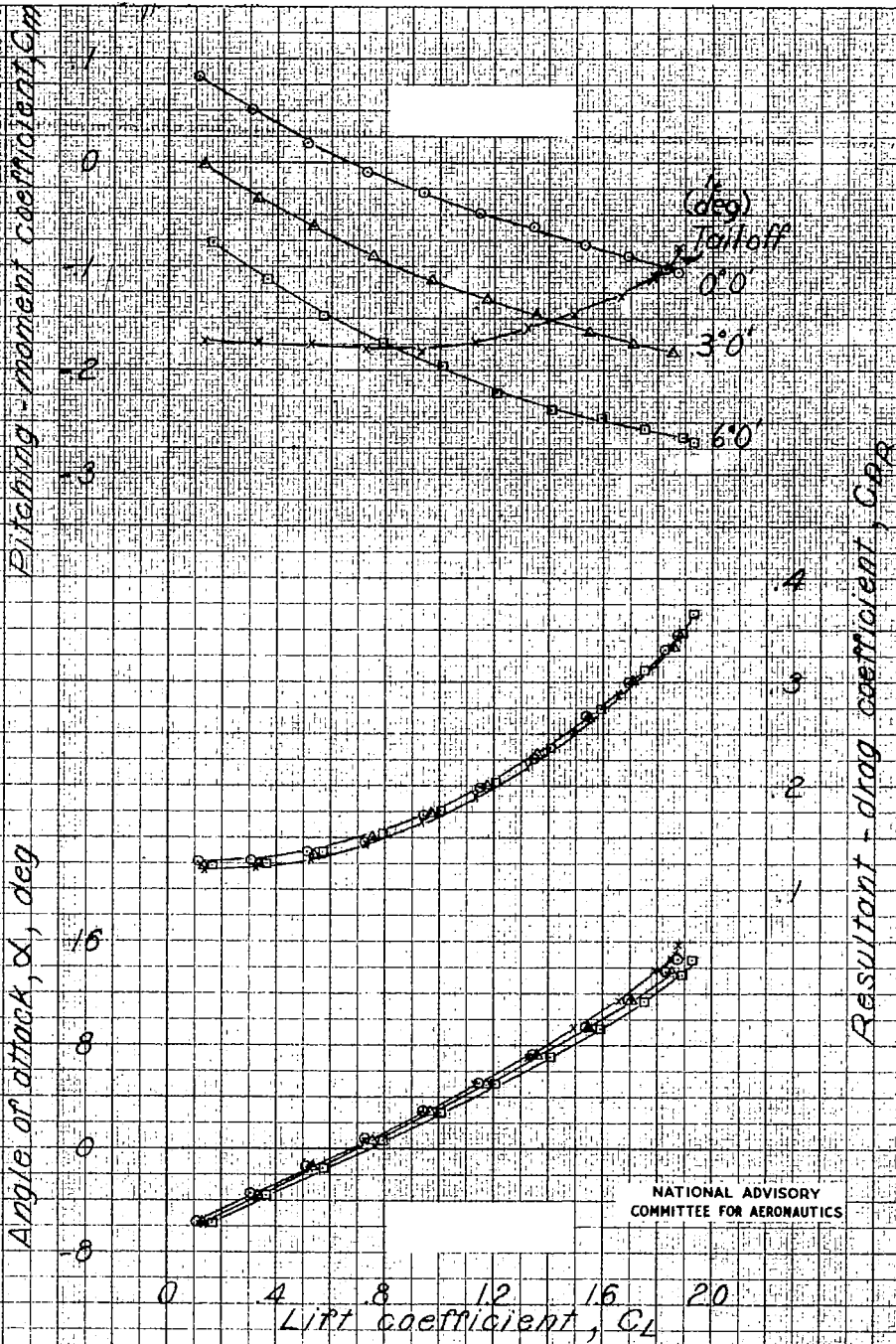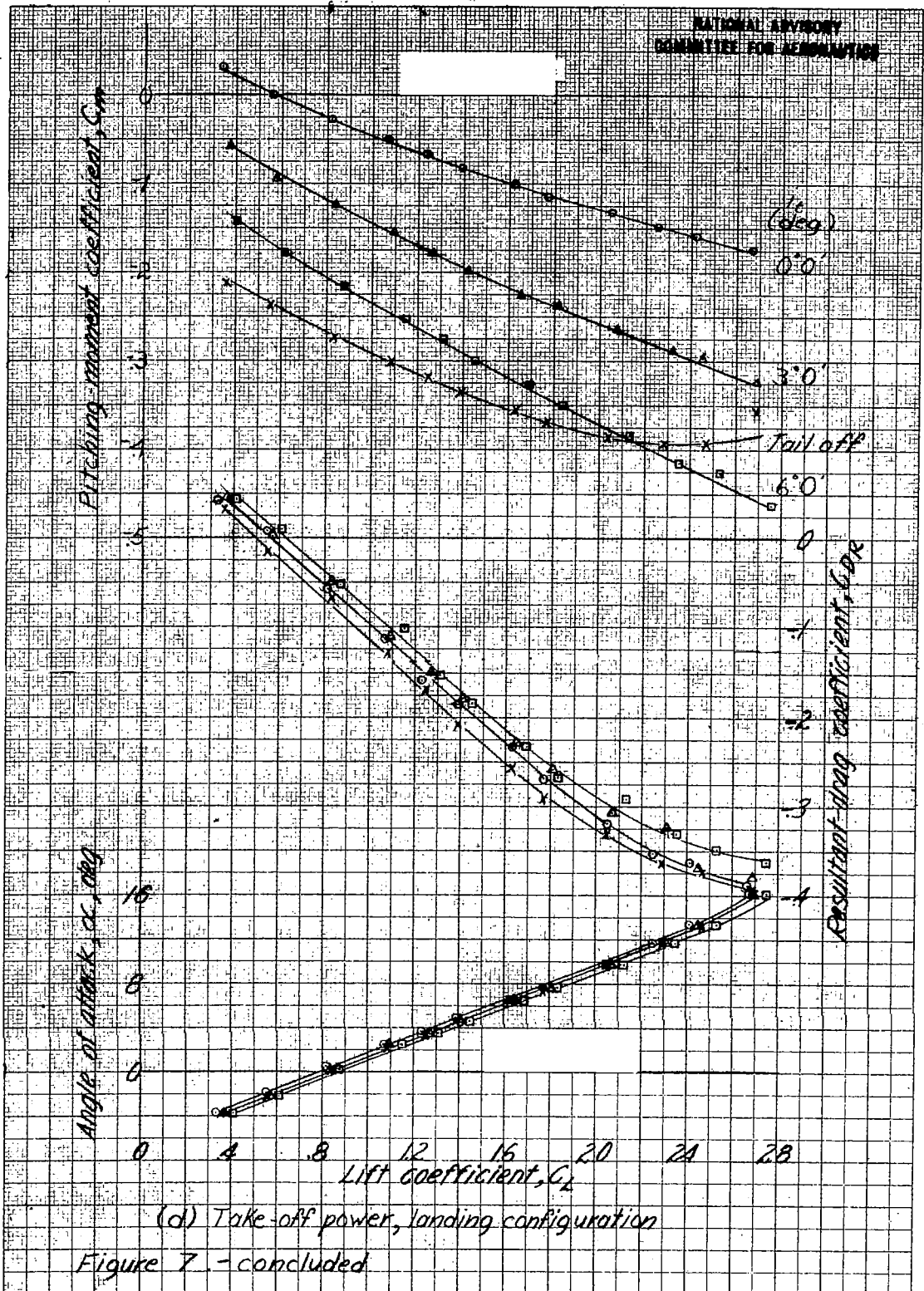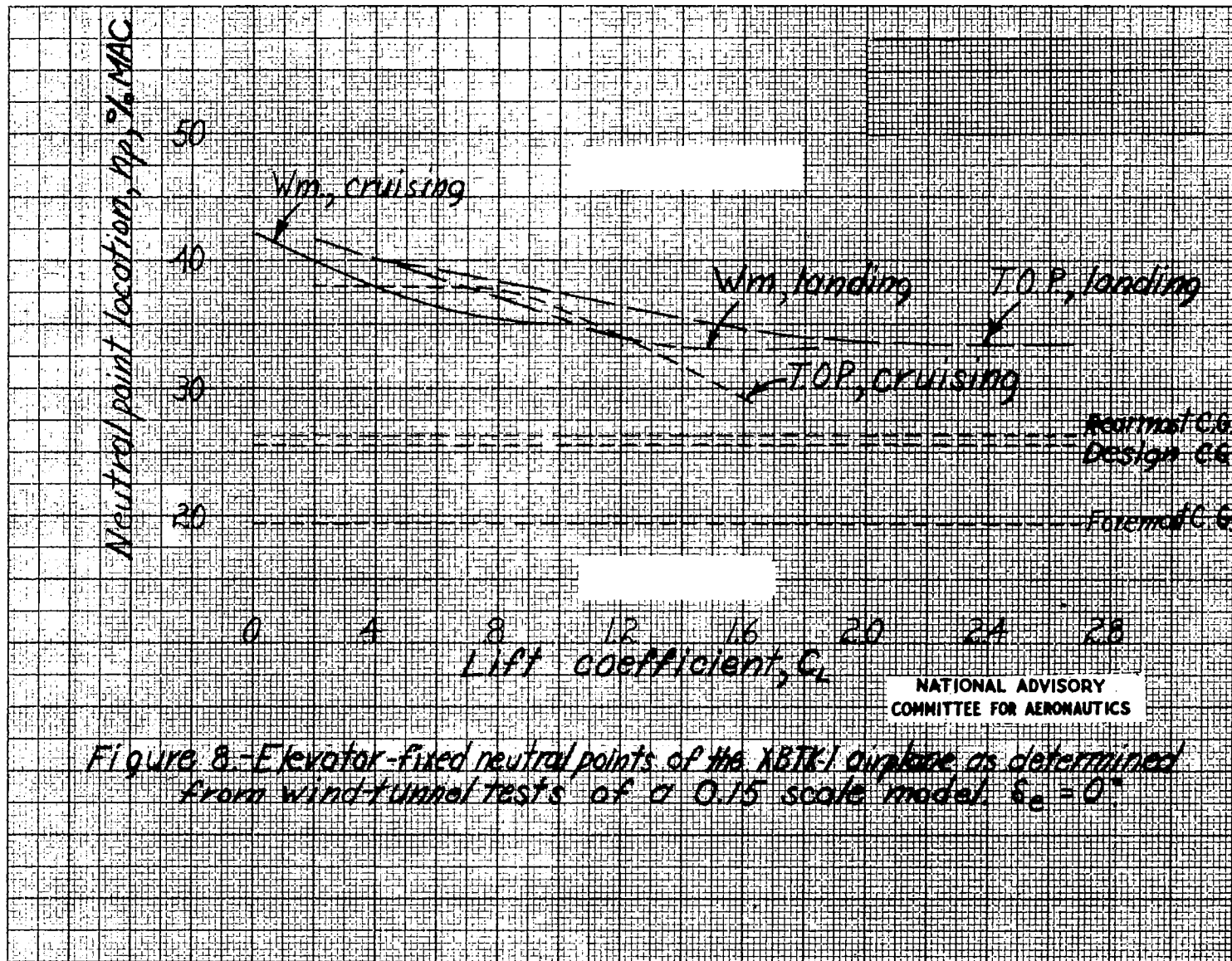
Figure 7 - concluded

Figure 8.-Elevator-fixed neutral points of the XBTK-1 airplane as determined from wind-tunnel tests of a 0.15 scale model. $\delta_e = 0°$

NATIONAL ADVISORY
COMMITTEE FOR AERONAUTICS
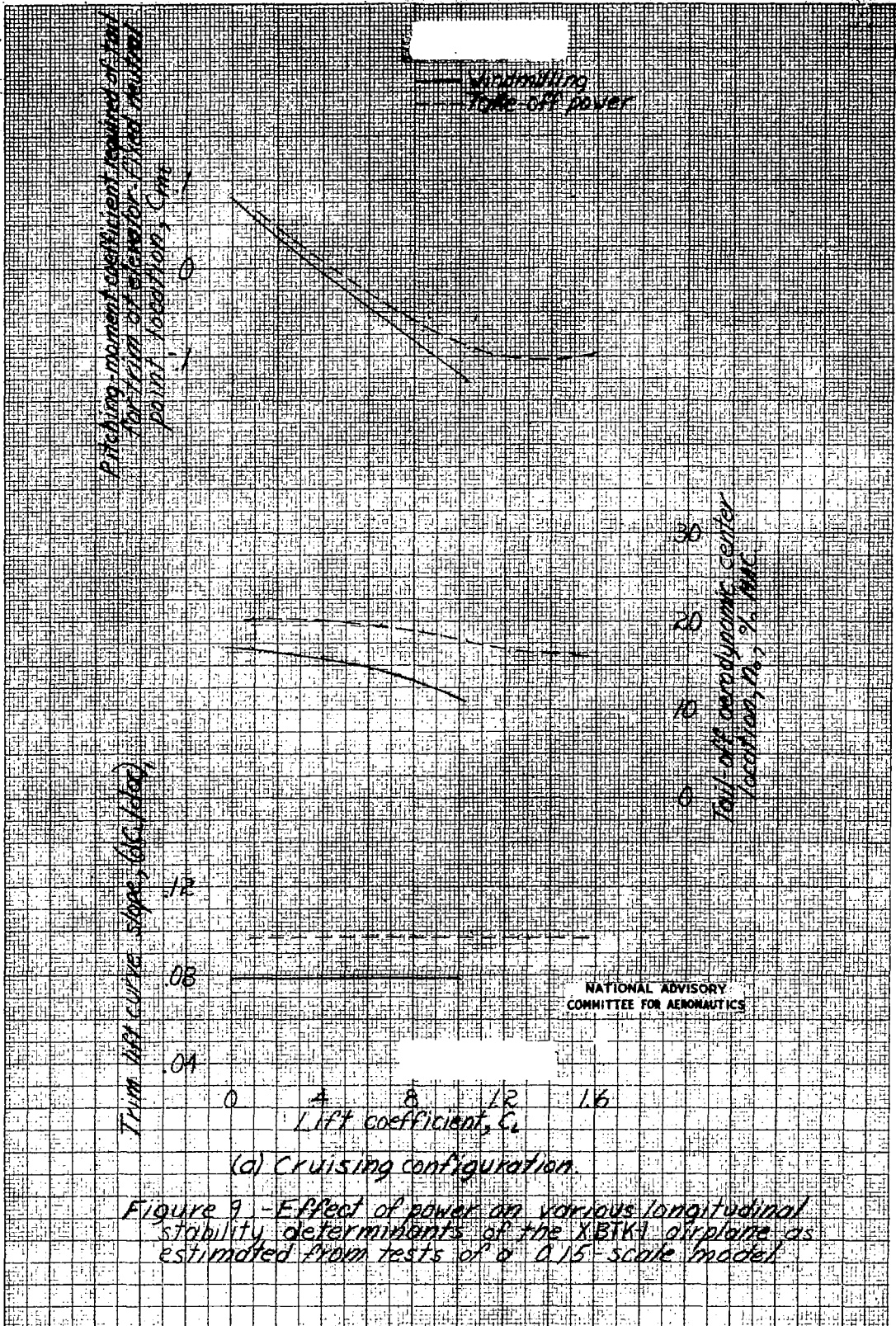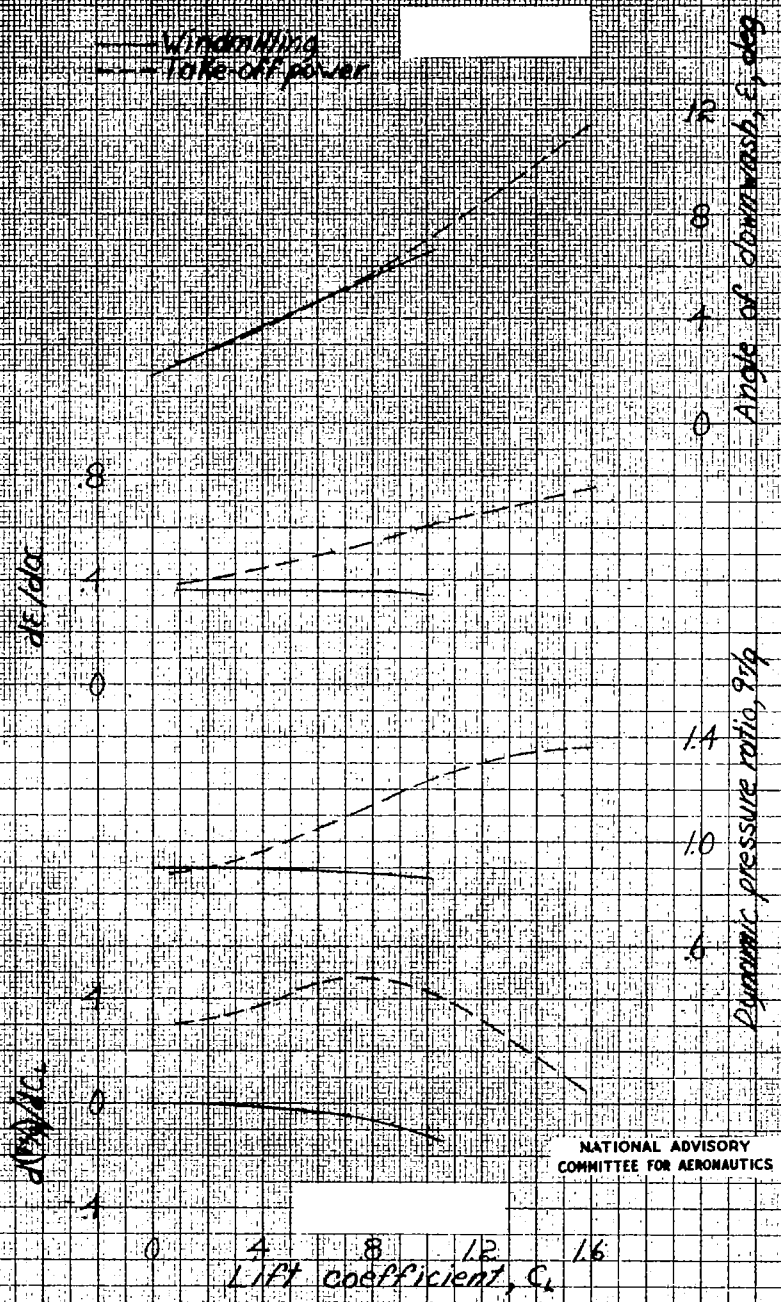
(a) Cruising configuration.

Figure 9.- Effect of power on various longitudinal stability determinants of the XBTK-1 airplane as estimated from tests of a 0.15-scale model.

(a) concluded

Figure 9.- continued

NATIONAL ADVISORY
COMMITTEE FOR AERONAUTICS
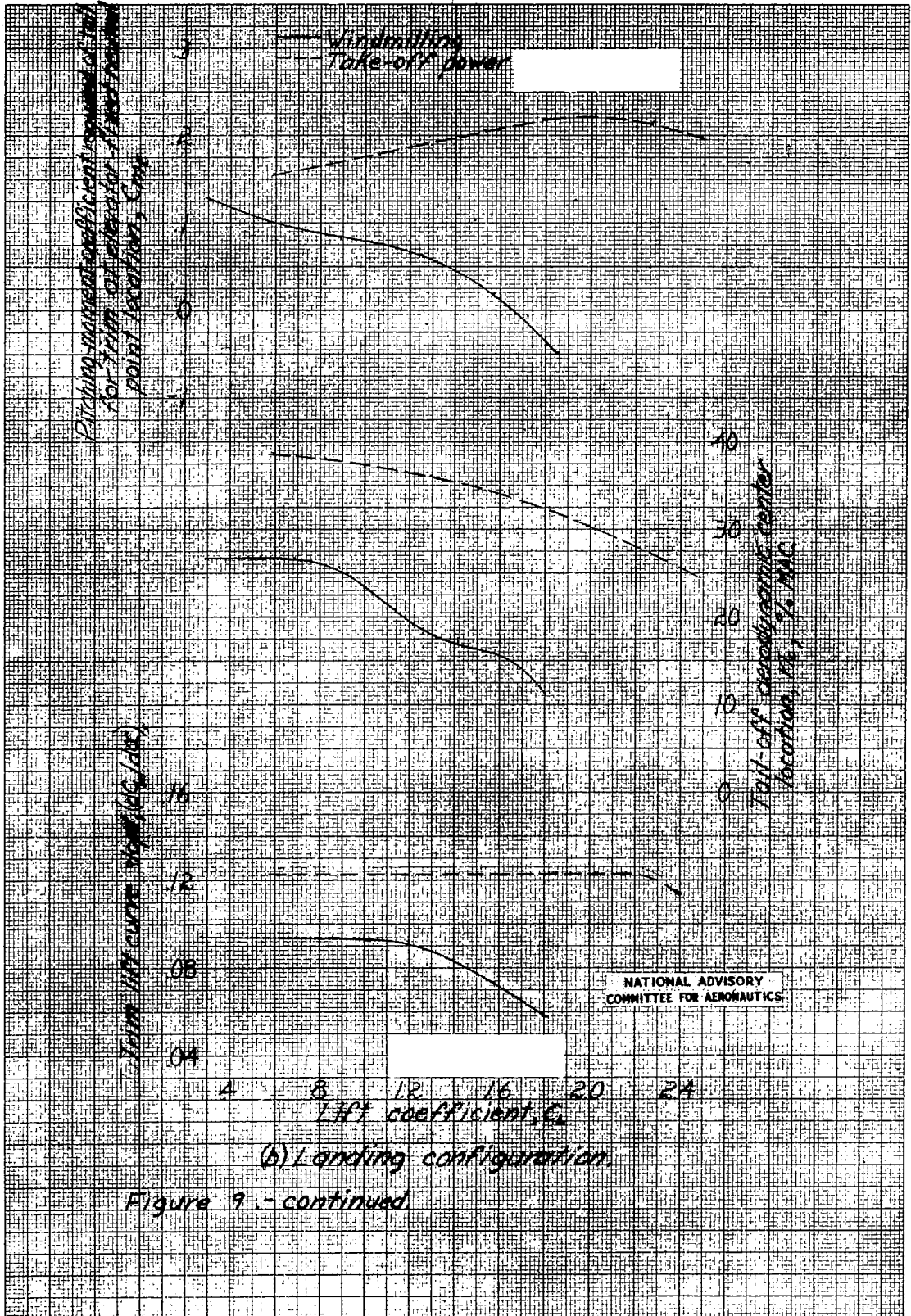
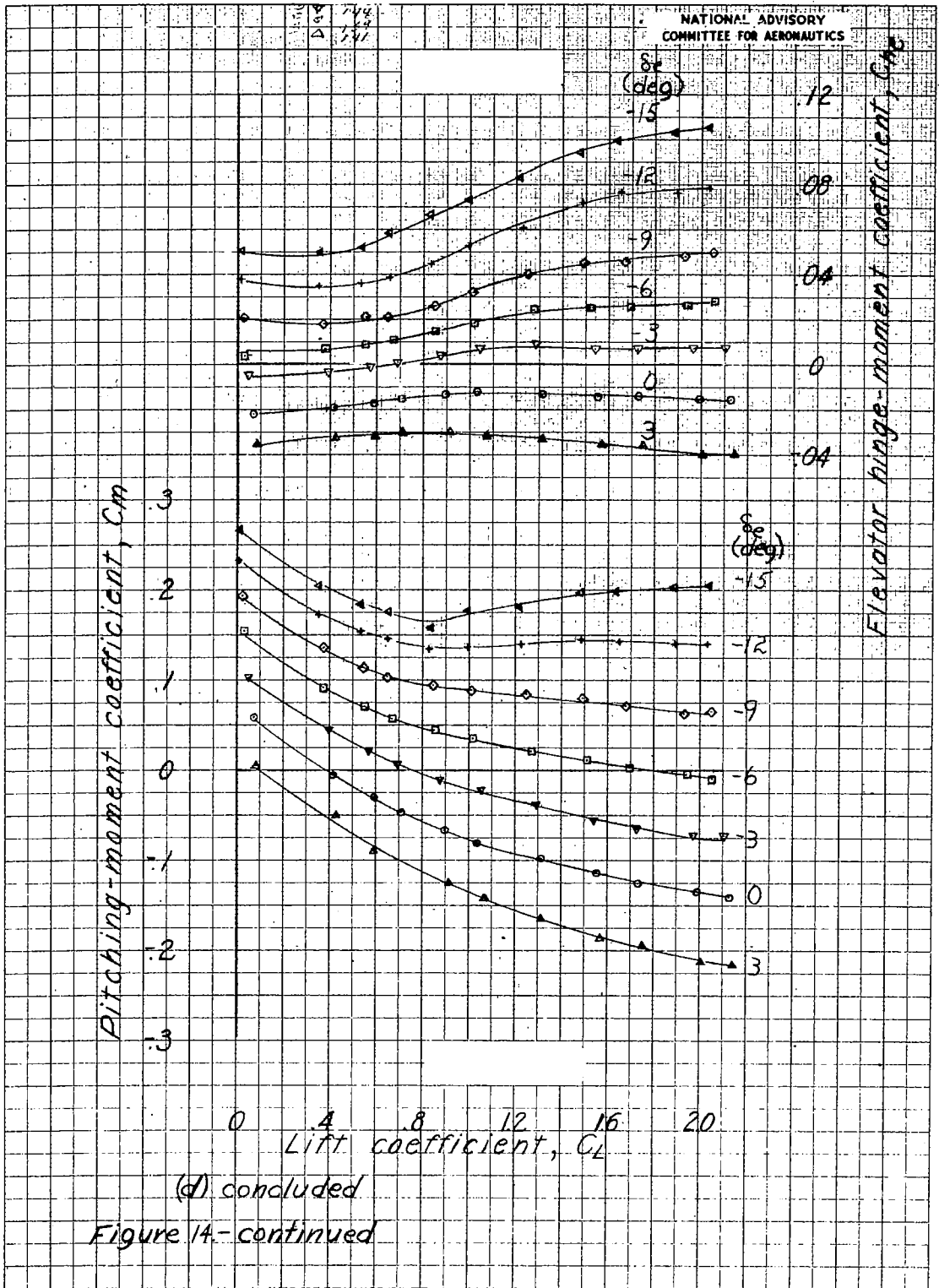(b) Landing configuration

Figure 9.- continued
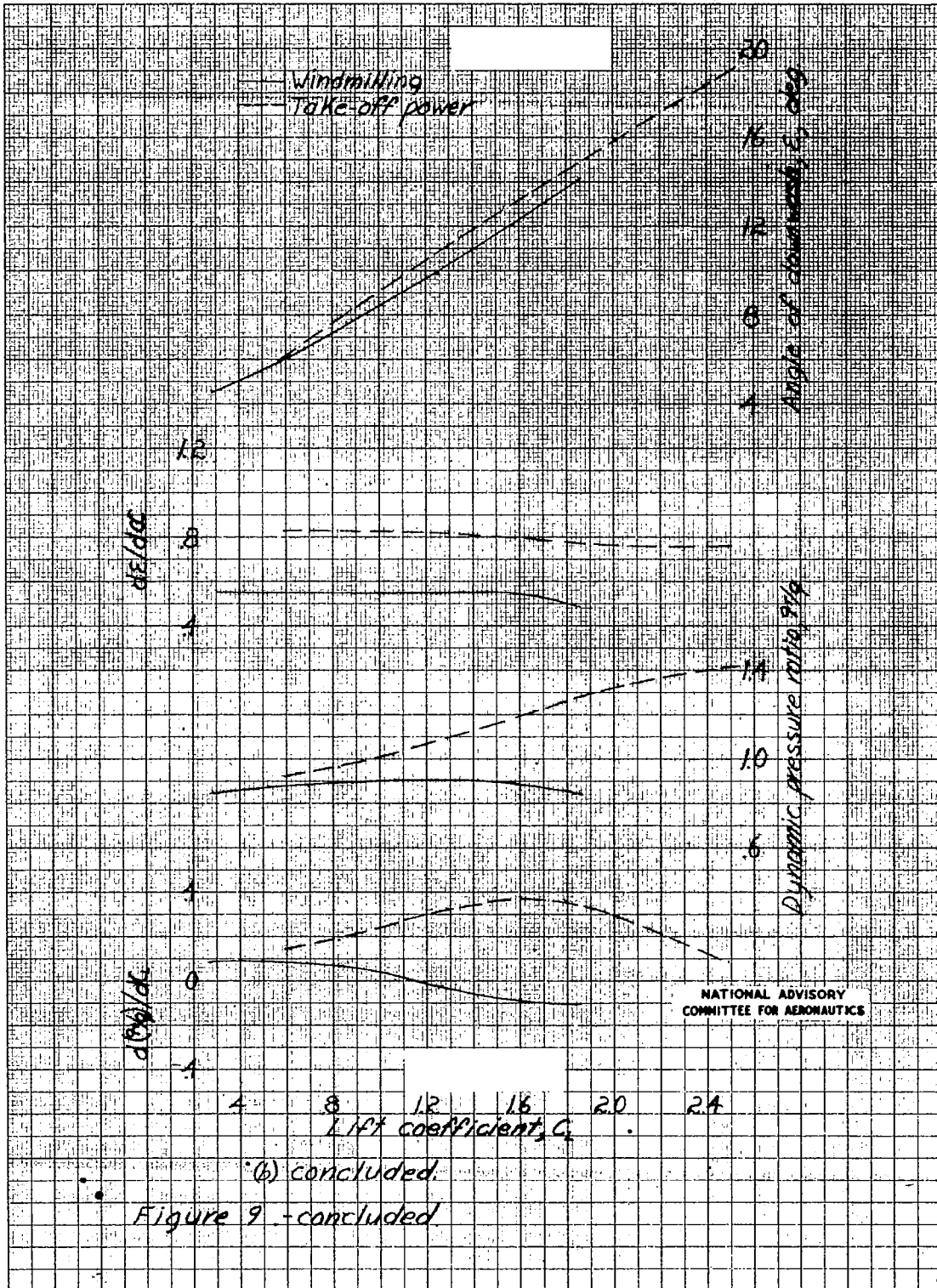
(b) concluded.

Figure 9 - concluded

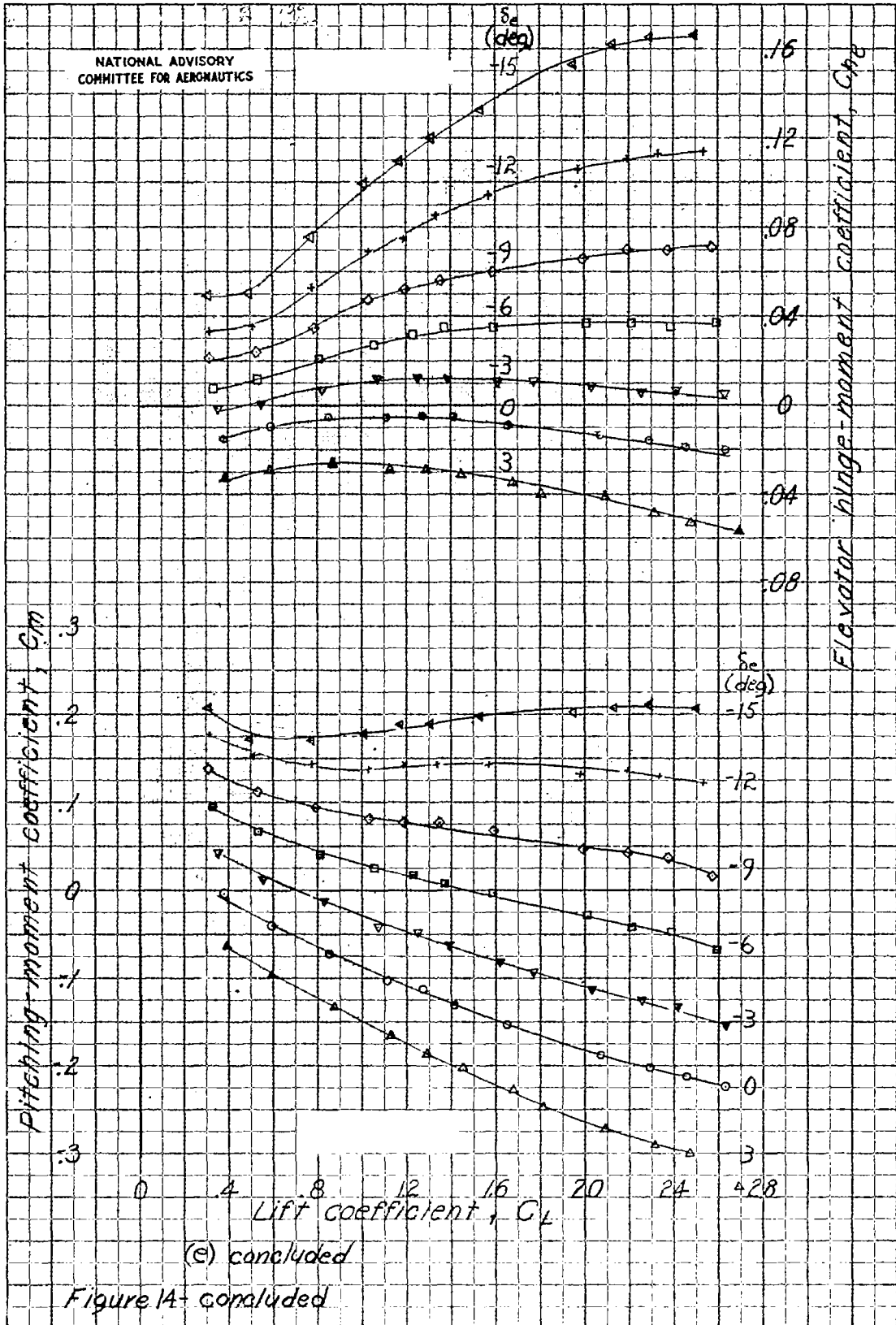(a) Windmilling, cruising configuration

Figure 10.- Effect of stabilizer on the aerodynamic characteristics in pitch of the 0.15 scale model of the XBTK airplane. δ_e, free

(b) Take-off power, cruising configuration

Figure 10.- Continued

NATIONAL ADVISORY
COMMITTEE FOR AERONAUTICS

(c) Windmilling landing configuration

Figure 10.- Continued

NATIONAL ADVISORY
COMMITTEE FOR AERONAUTICS
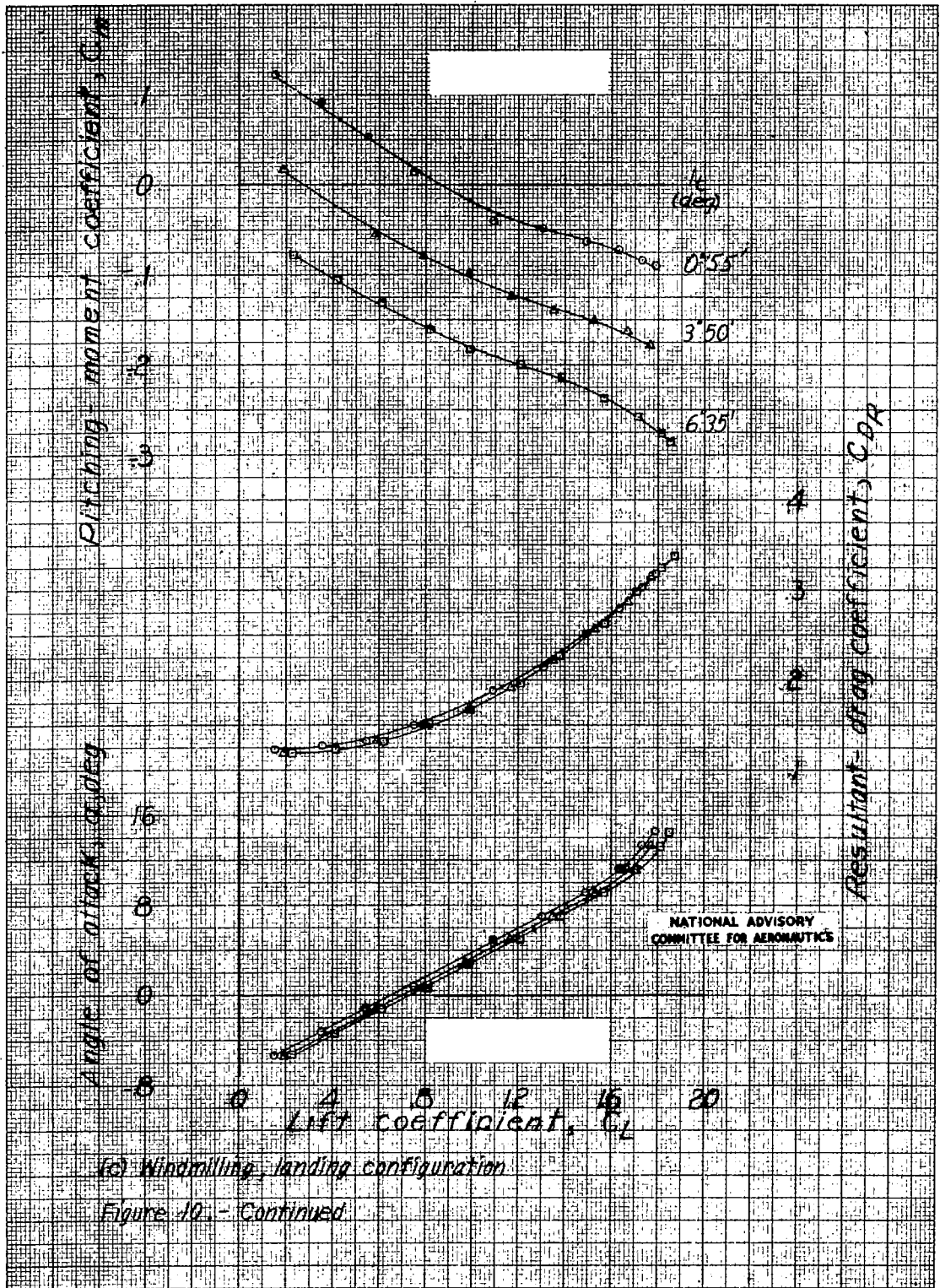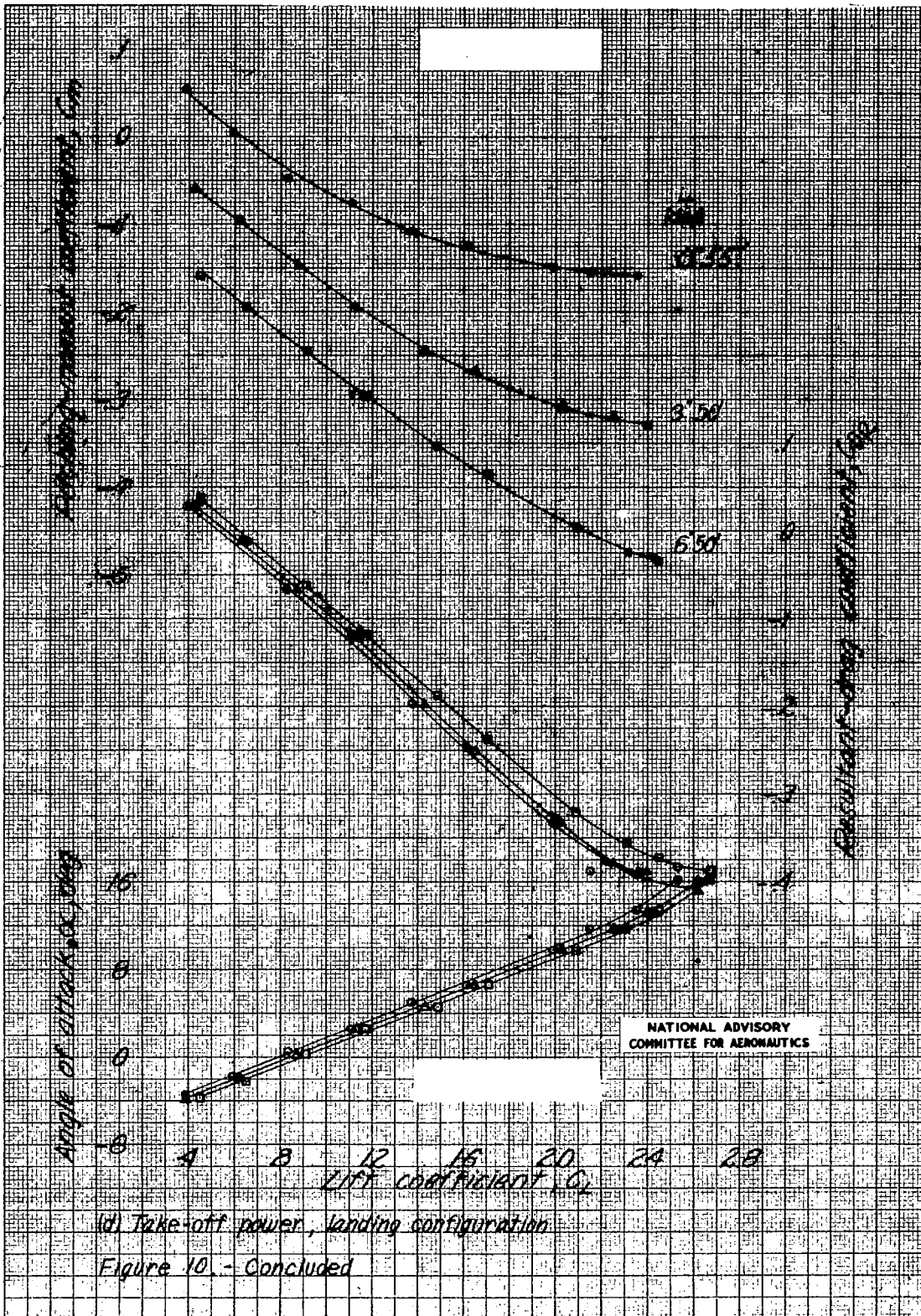
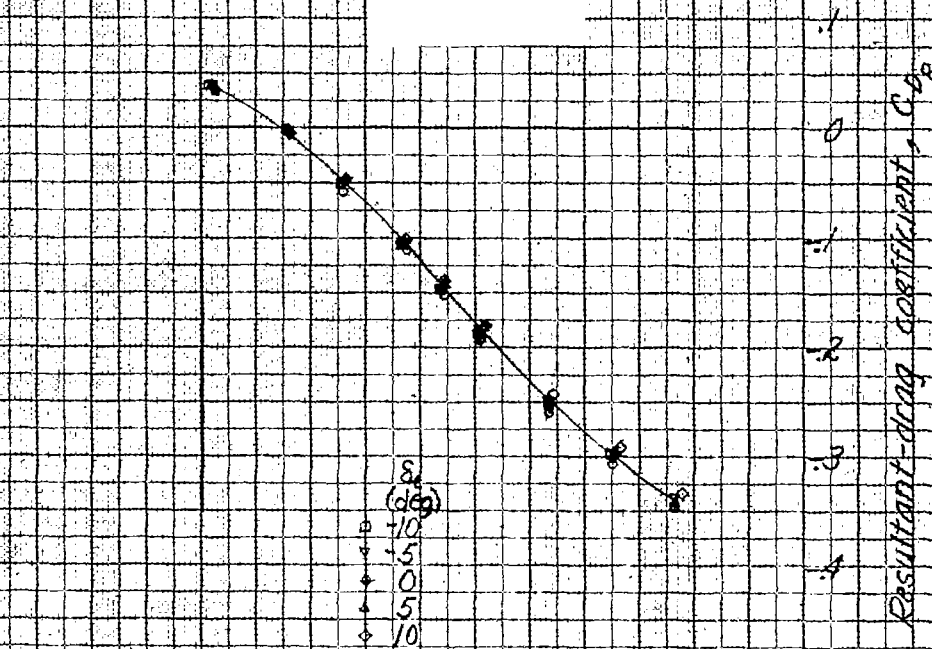(d) Take-off power, landing configuration

Figure 10.- Concluded
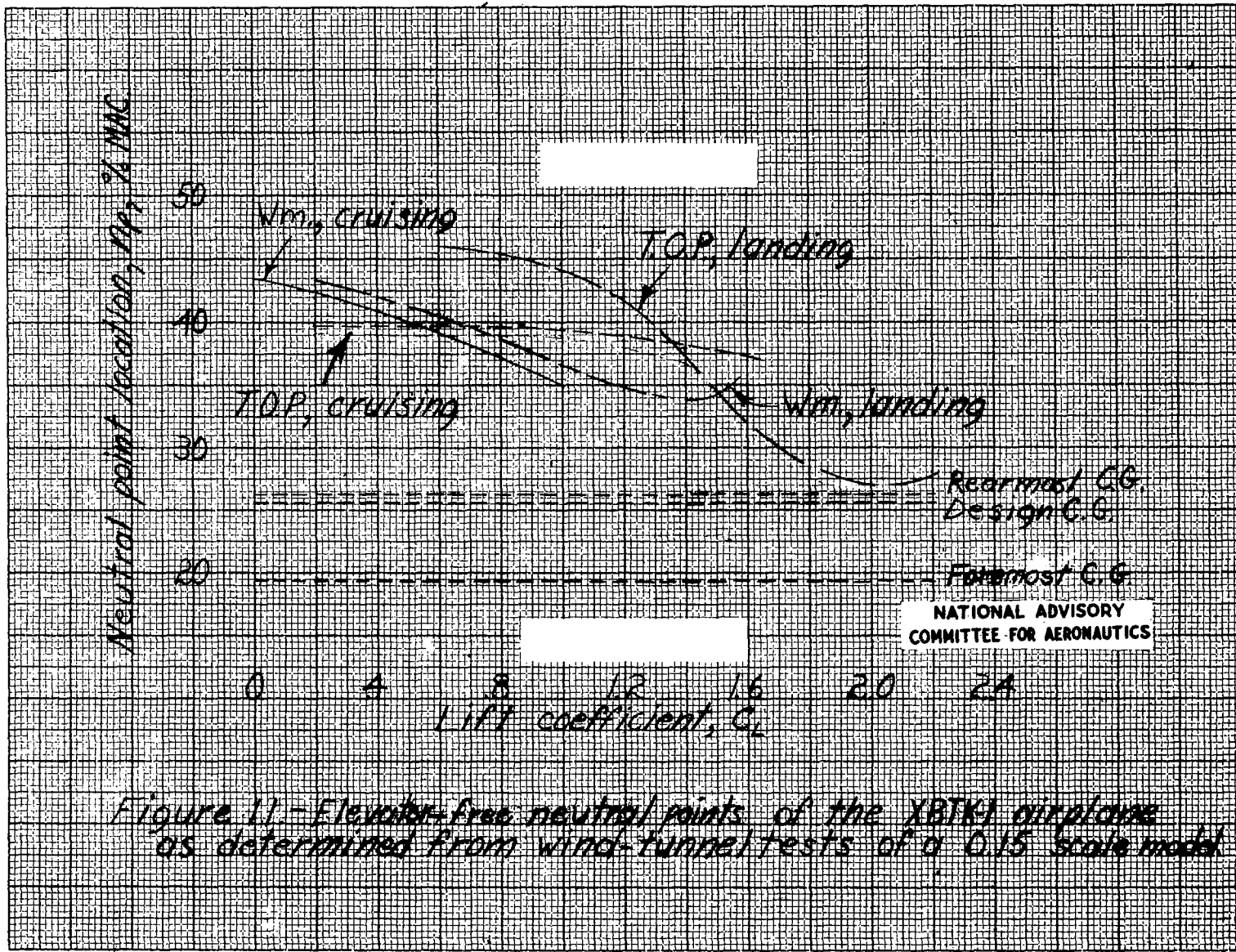
NATIONAL ADVISORY
COMMITTEE FOR AERONAUTICS

Figure II - Elevator-free neutral points of the XBTK1 airplane as determined from wind-tunnel tests of a 0.15 scale model.
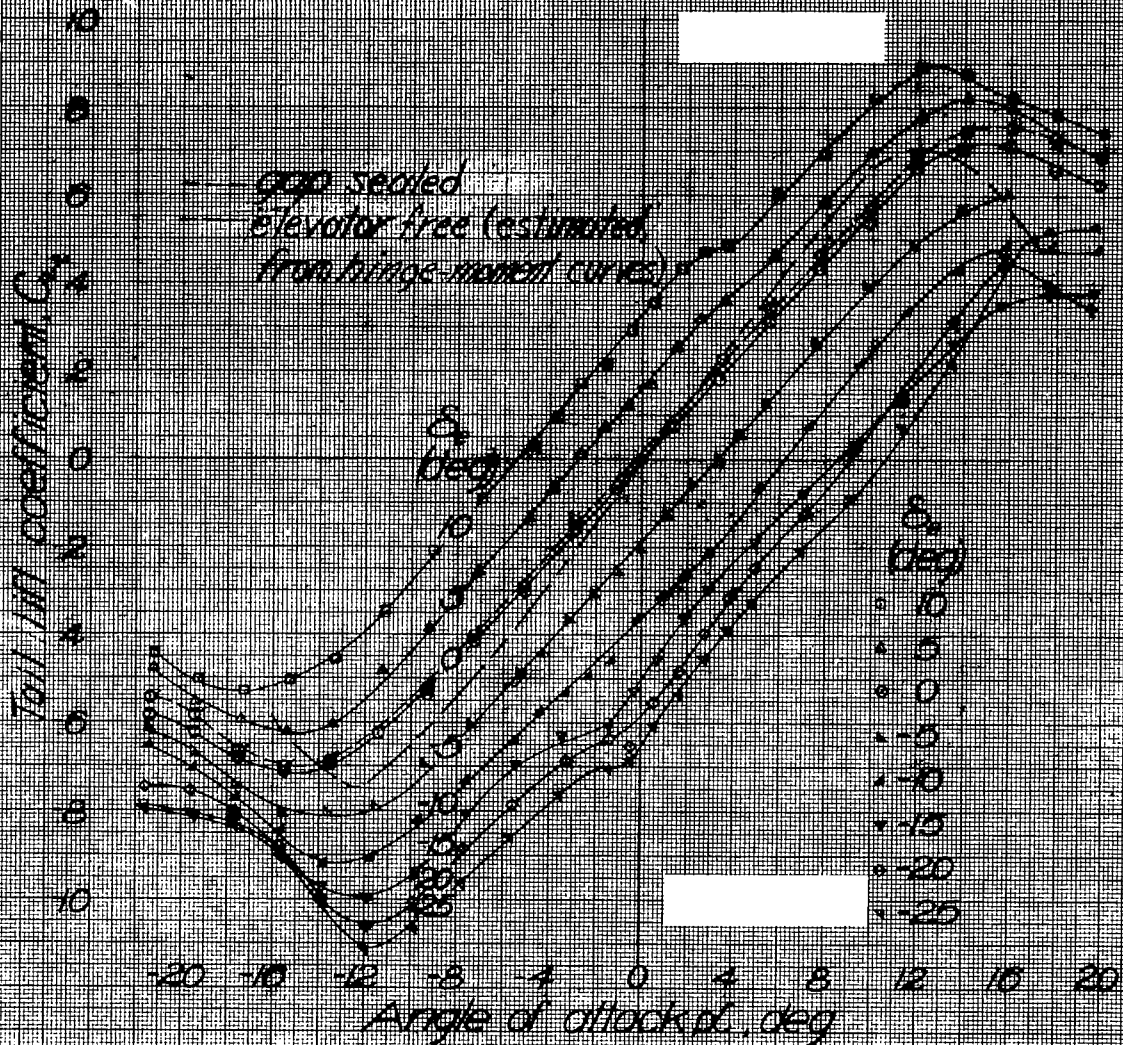
Figure 12.- Effect of elevator deflection on the aerodynamic characteristics of the isolated horizontal tail of 0.15-scale model of Fleetwings XBTK-1 airplane, $\delta_f = 0°$.

Figure 12.- Concluded.

Figure 13.- Effect of tab deflection on the aerodynamic characteristics of the isolated horizontal tail of 0.15-scale model of Fleetwings XBTK-1 airplane. $\delta_e = 0°$.
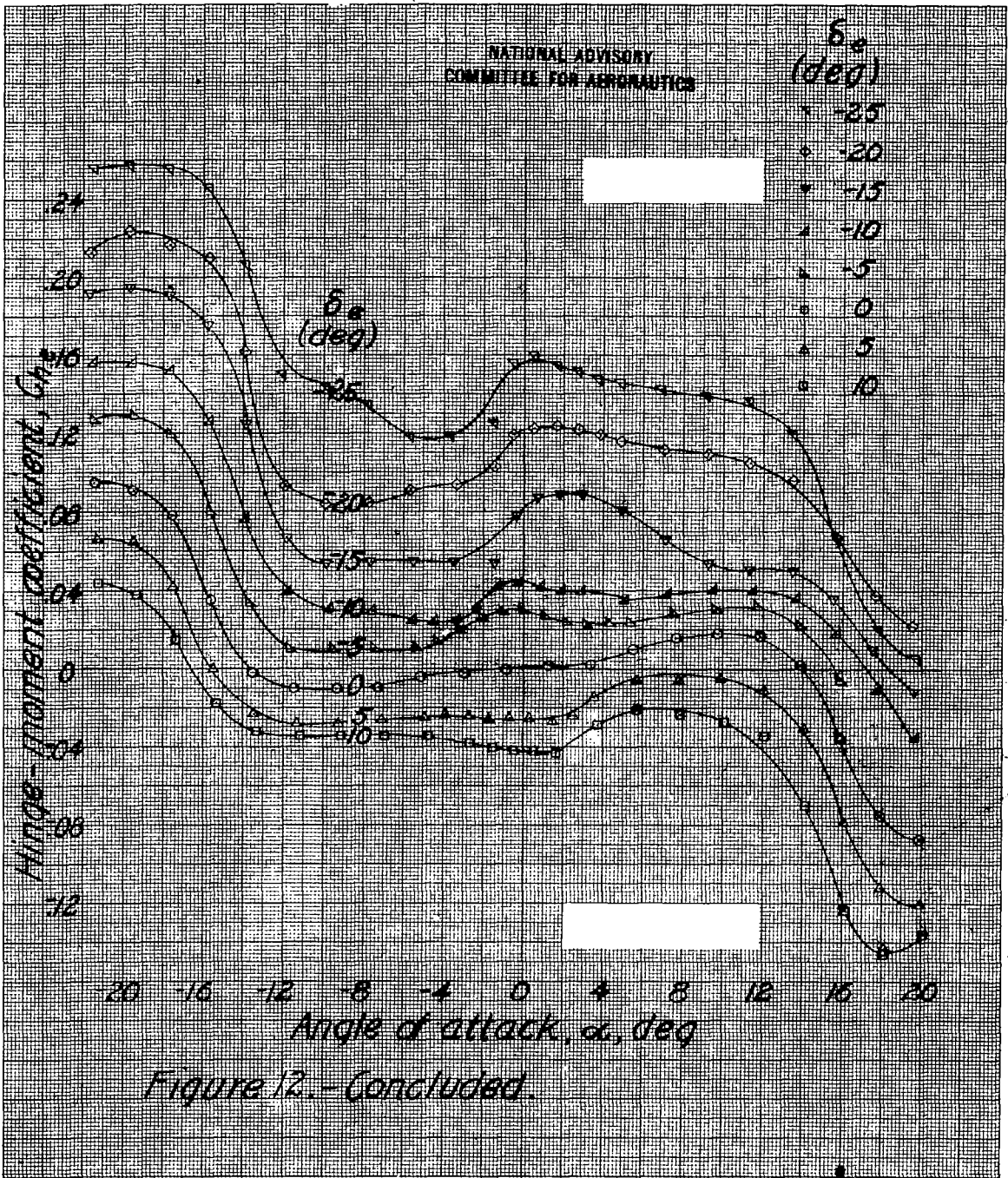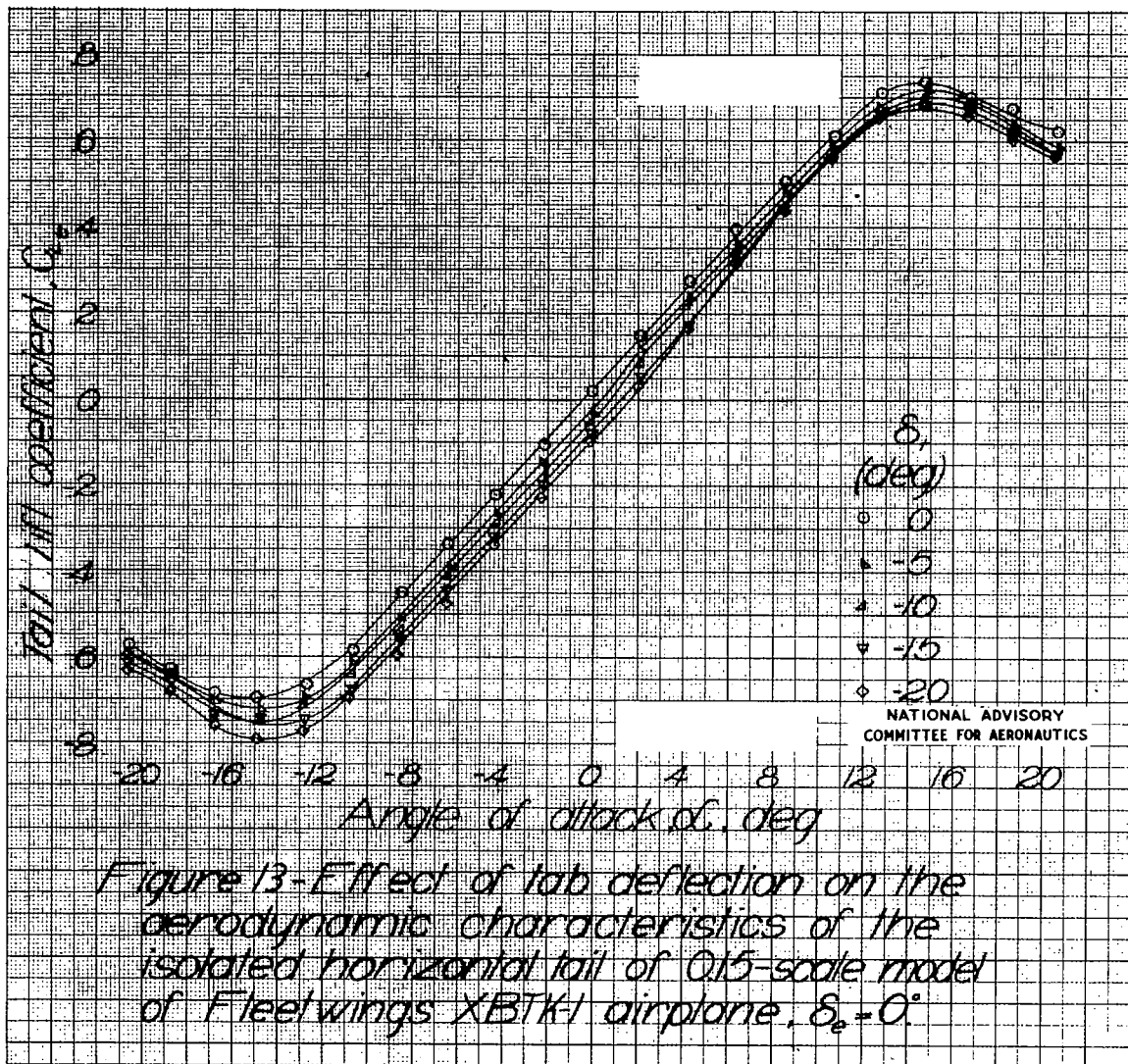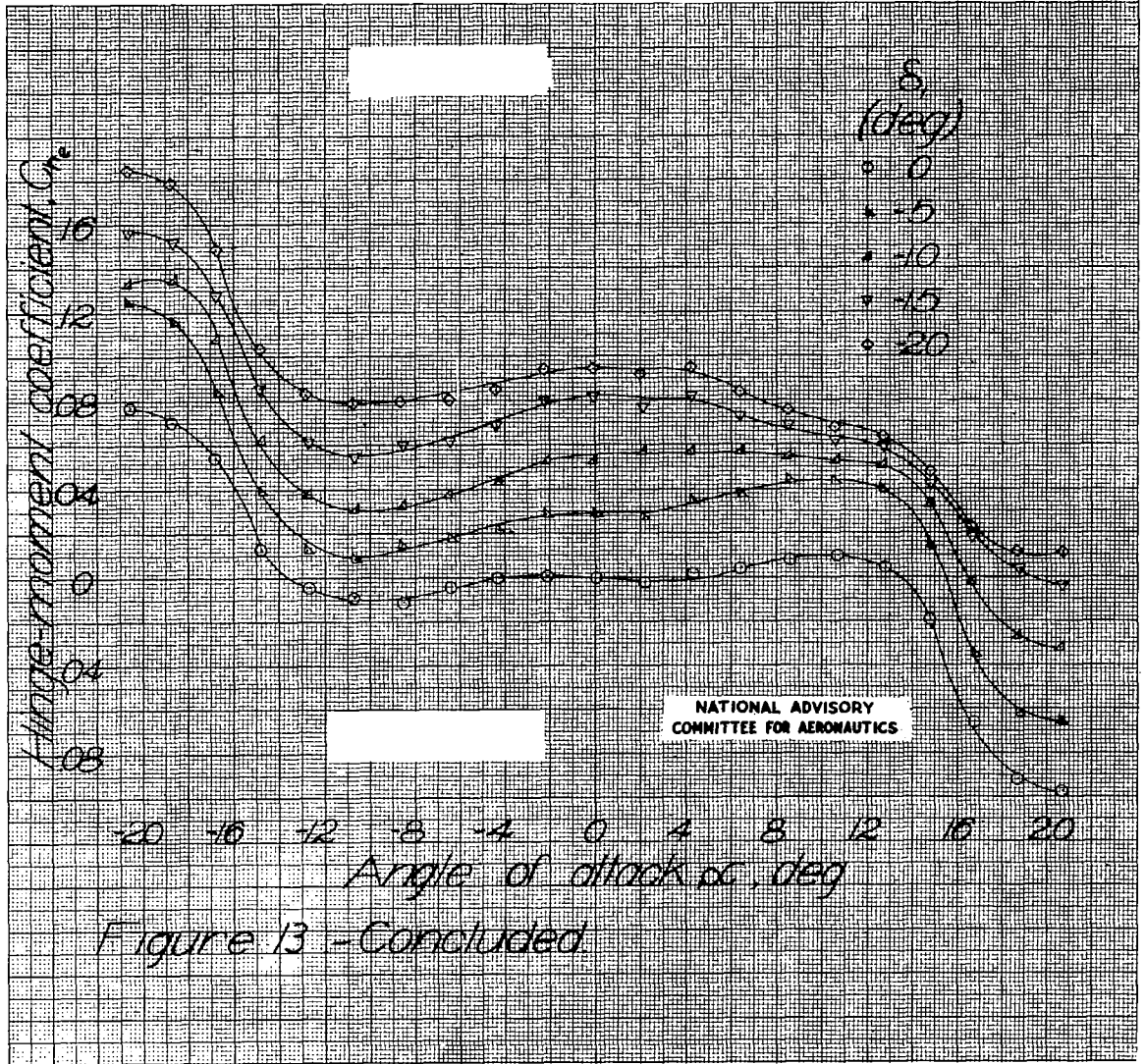
Figure 13 .- Concluded

NATIONAL ADVISORY
COMMITTEE FOR AERONAUTICS

Resultant-drag coefficient, C_{DR}

δ_e
(deg)
3
0
-3
-6
-9
-12
-15
-20

Angle of attack, α, deg

24

16

8

0

-8

-4   0   4   8   12   16

Lift coefficient, C_L
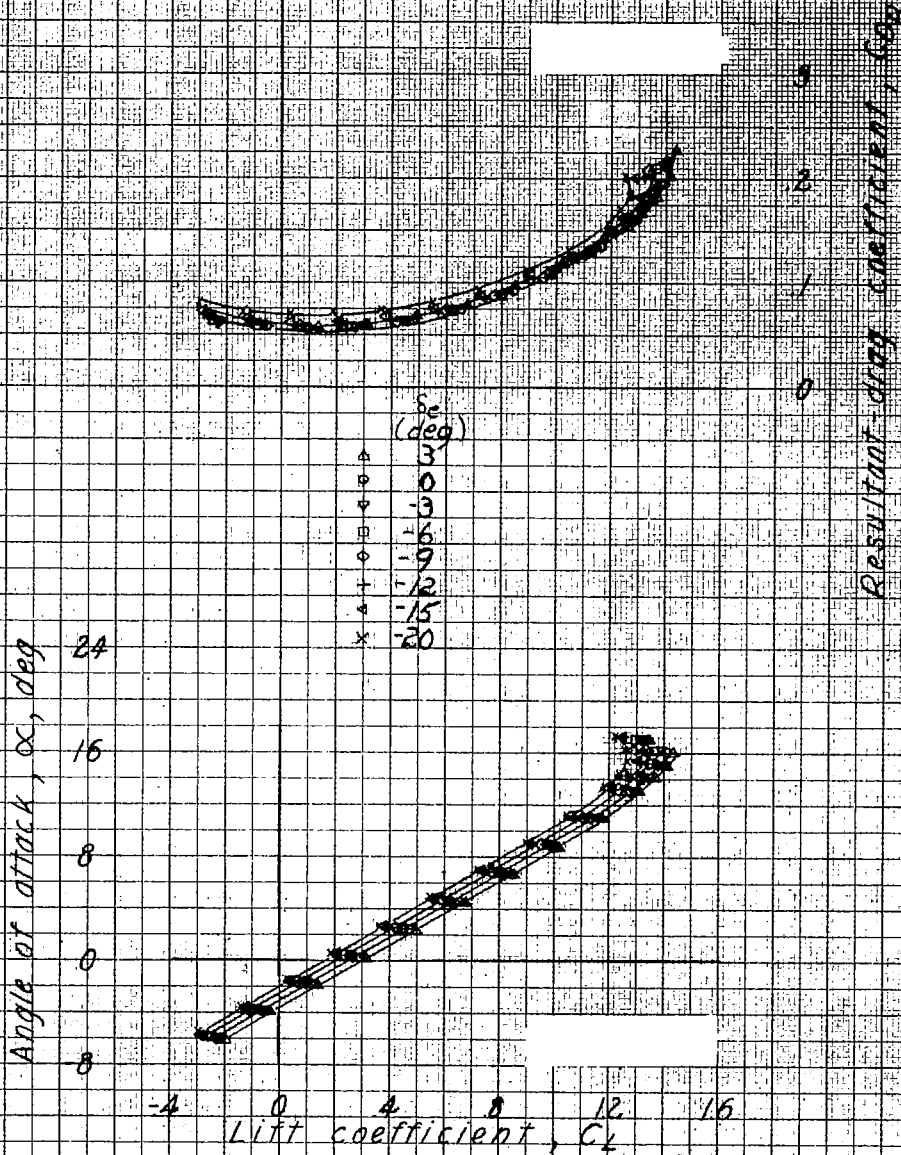
(a) Windmilling, cruising configuration

Figure 14 – Effect of elevator deflection on the aerodynamic characteristics in pitch of the 0.15-scale model of the XBTK-1 airplane. $\delta_f = 0°$, $i_t = 1°0'$
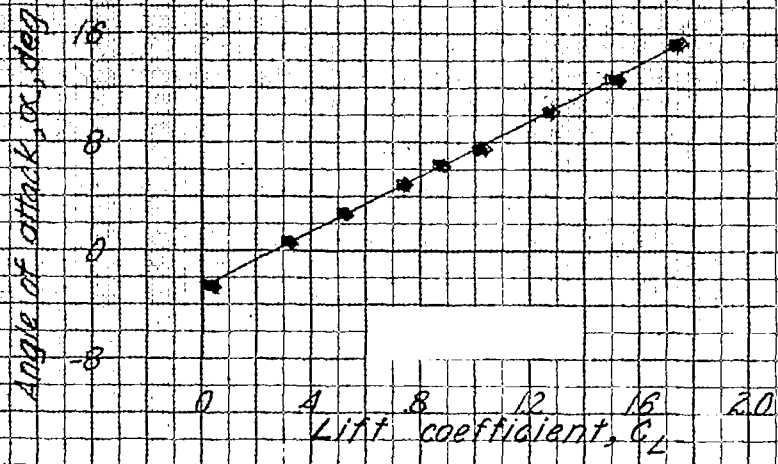
(a) concluded

Figure 14.- continued

NATIONAL ADVISORY
COMMITTEE FOR AERONAUTICS

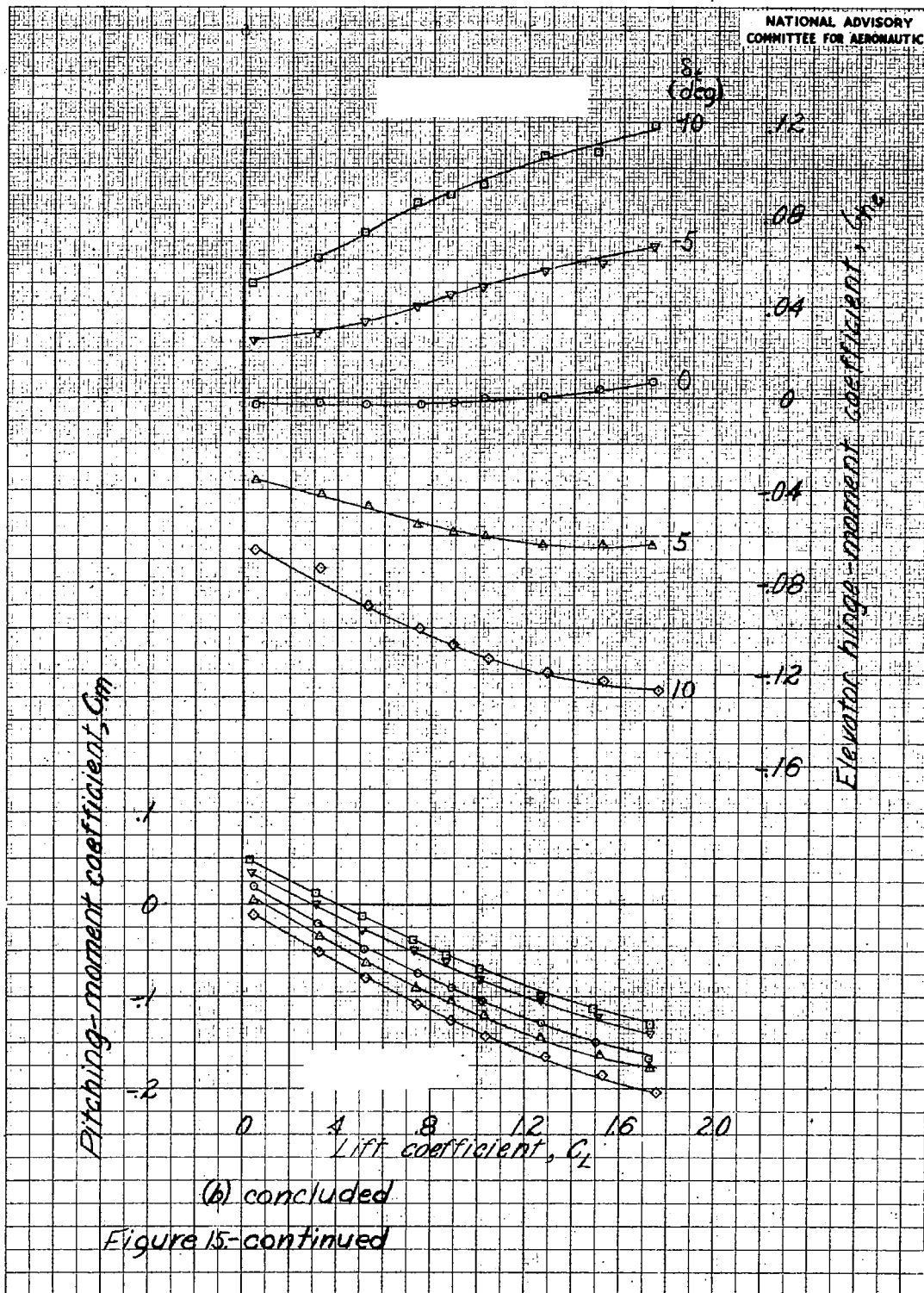Resultant-drag coefficient, c_{DR}

Angle of attack, α, deg

δ_e
(deg)

Lift coefficient, c_L

(b) Take-off power, cruising configuration

Figure 14.- continued

MR No. L5D27a

NATIONAL ADVISORY
COMMITTEE FOR AERONAUTICS

(b) concluded

Figure 14.- continued

(c) windmilling, landing configuration

Figure 14. - continued

(c) concluded

Figure 14 – continued
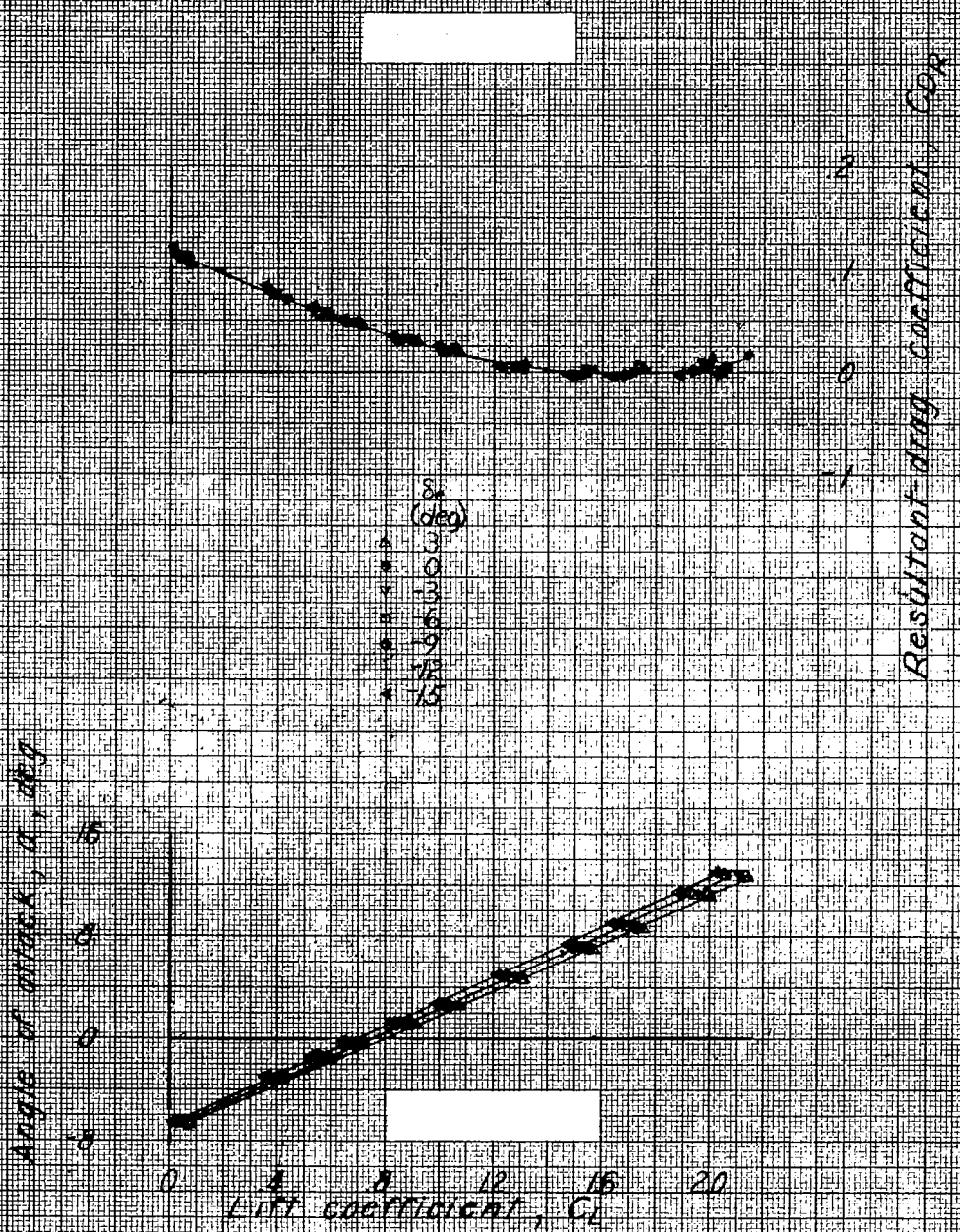
(d) 60 percent rated power, landing configuration

Figure 14.- continued

NATIONAL ADVISORY
COMMITTEE FOR AERONAUTICS

(d) concluded

Figure 14.- continued

(e) concluded

Figure 14- concluded

NATIONAL ADVISORY
COMMITTEE FOR AERONAUTICS
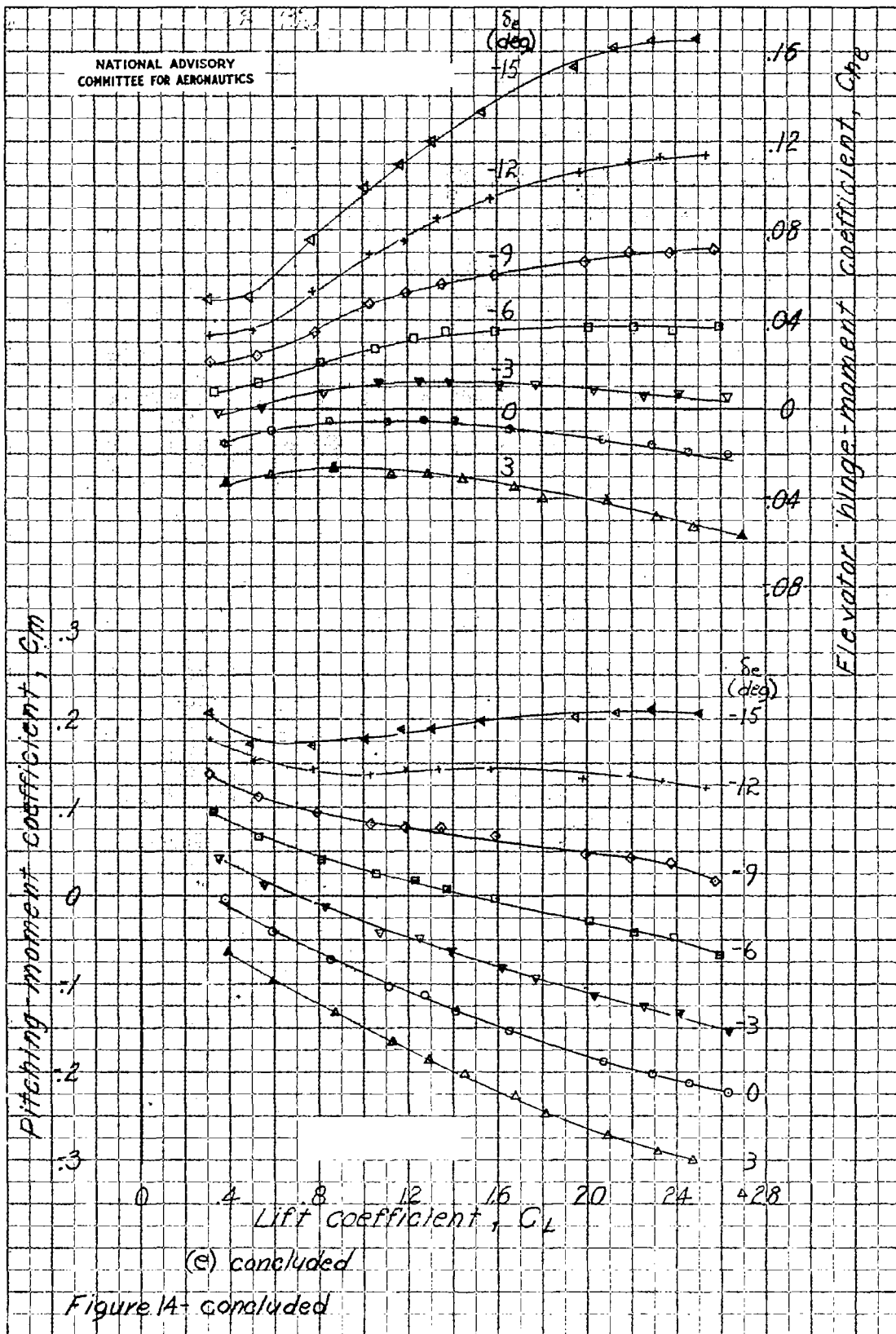
(c) concluded

Figure 14.- concluded
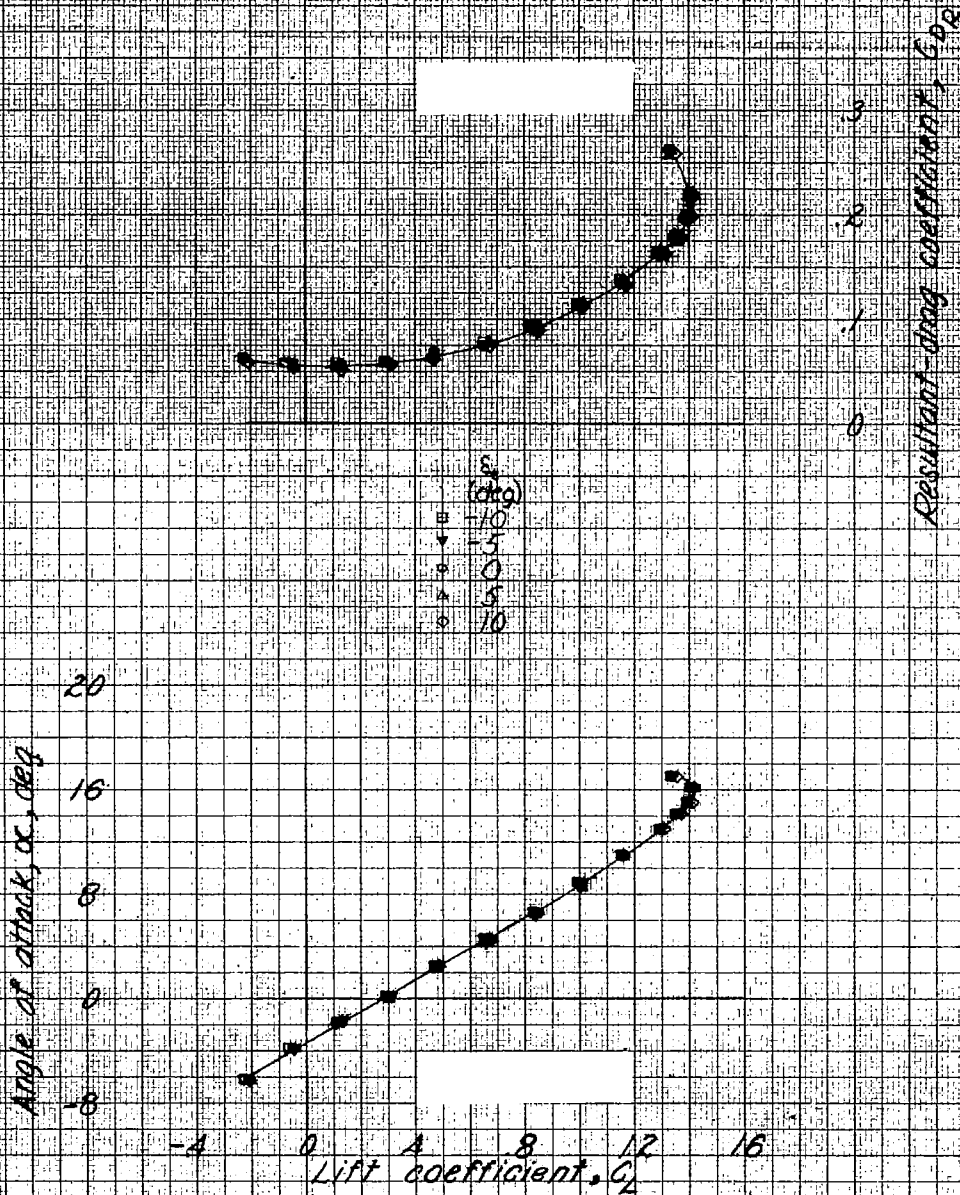
(a) Windmilling, cruising configuration

Figure 15.- Effect of elevator tab deflection on the aero-
dynamic characteristics in pitch of the 0.15-scale
model of the XBTK-1 airplane. $\delta_e = 0°$, $i_t = 1°0'$
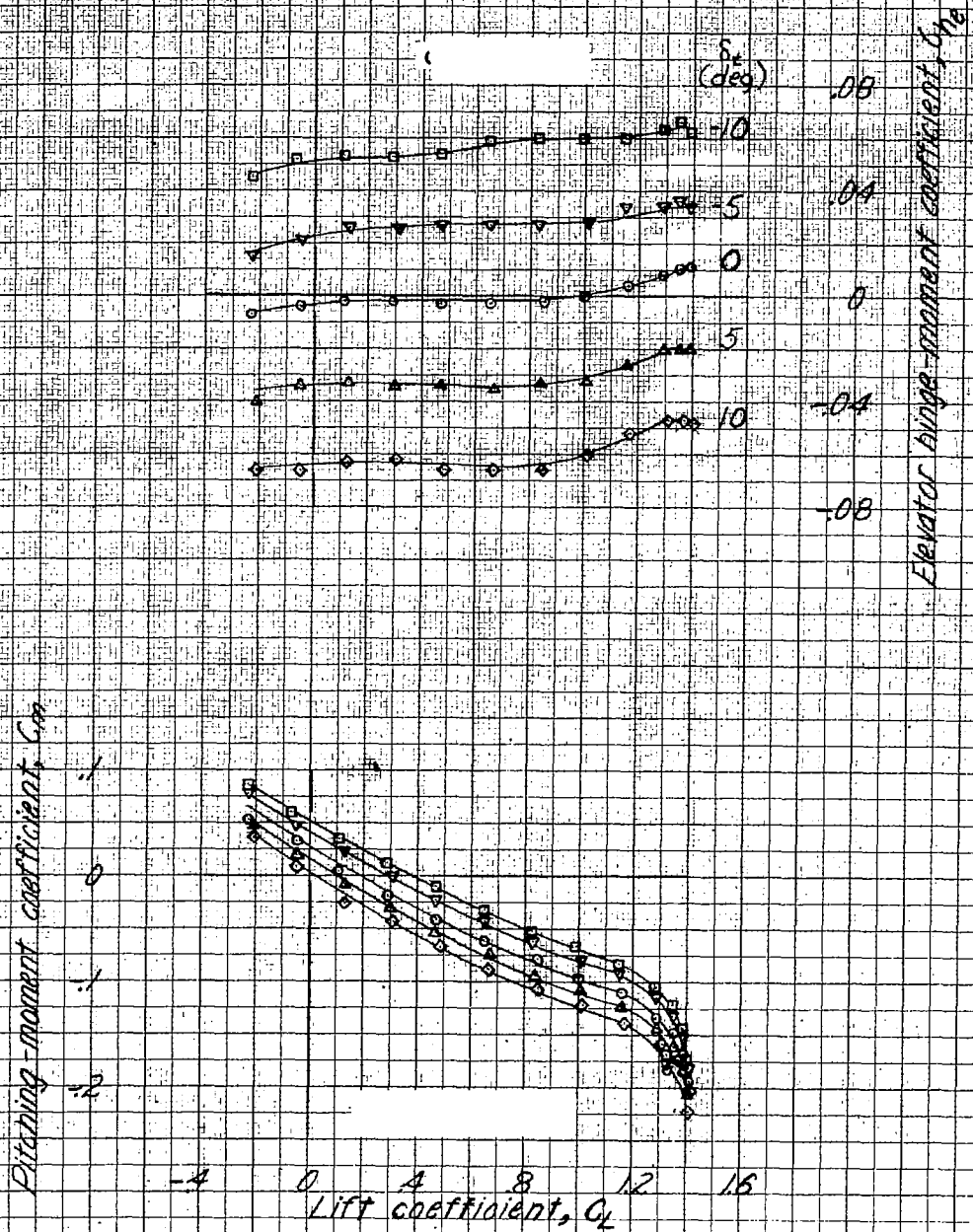
(a) concluded

Figure 15.- continued

(b) Take-off power, cruising configuration

Figure 15.- continued

(b) concluded

Figure 15 - continued

NATIONAL ADVISORY
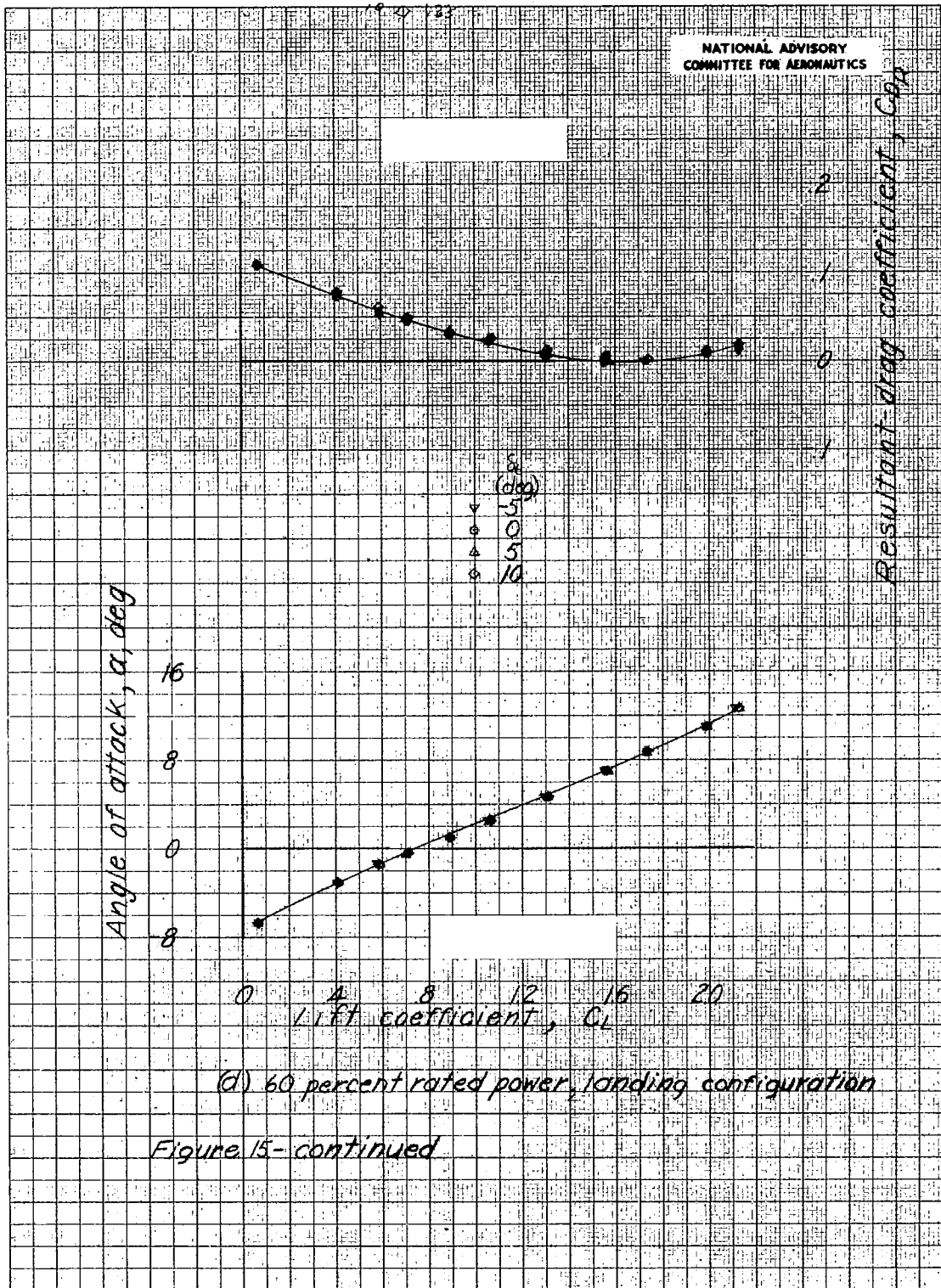COMMITTEE FOR AERONAUTICS

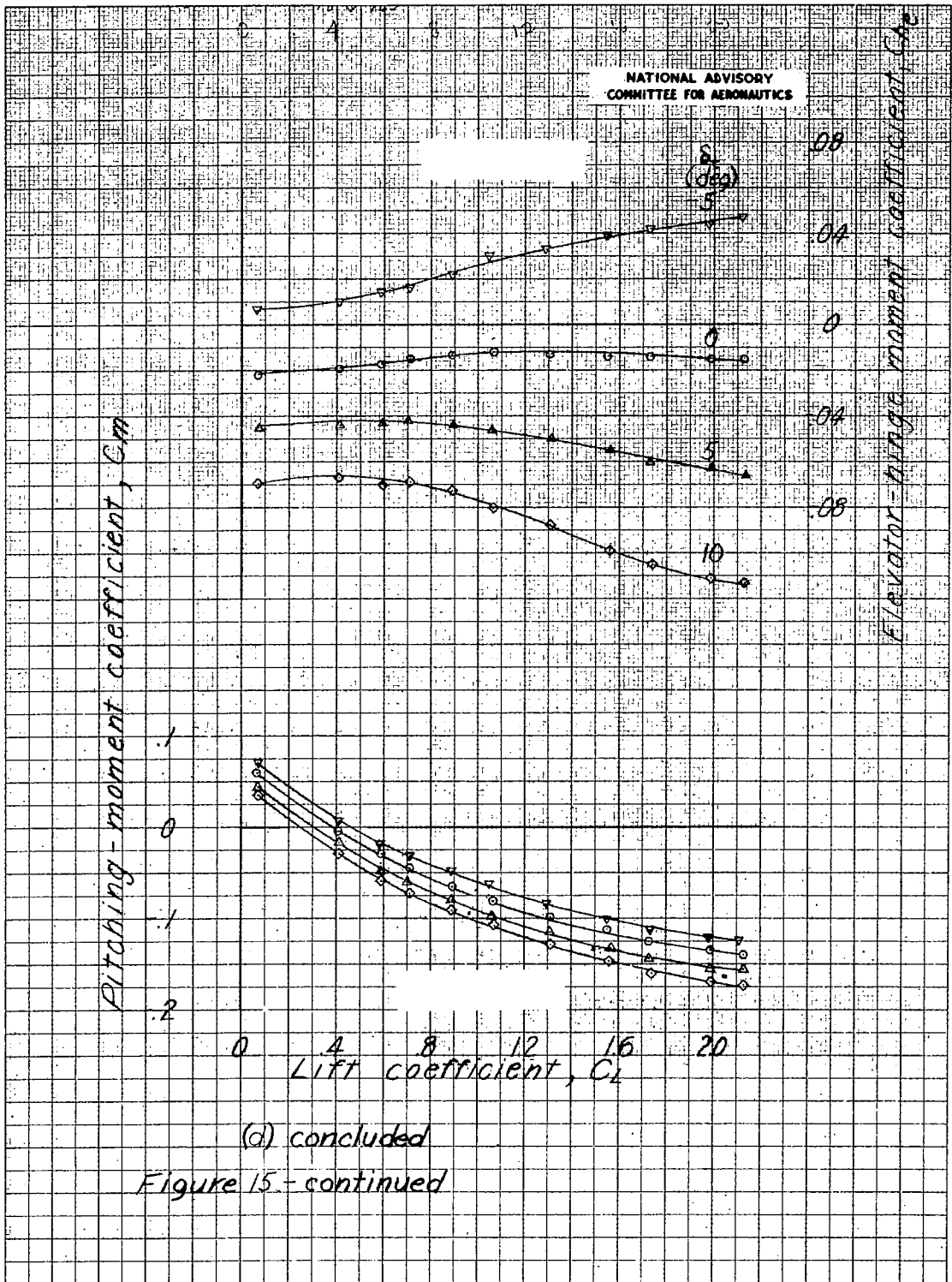(b) Take-off power, cruising configuration

Figure 15.- continued

(b) concluded

Figure 15.-continued

NATIONAL ADVISORY
COMMITTEE FOR AERONAUTICS

Resultant-drag coefficient, C_{D_R}

Angle of attack, α, deg

δ_t
(deg)
-5
0
5
10

Lift coefficient, C_L

(c) Windmilling, landing configuration

Figure 15.- continued

NATIONAL ADVISORY
COMMITTEE FOR AERONAUTICS

Elevator hinge-moment coefficient, C_h

Pitching-moment coefficient, C_m

Lift coefficient, C_L

(c) concluded

Figure 15.- continued.

(d) 60 percent rated power, landing configuration
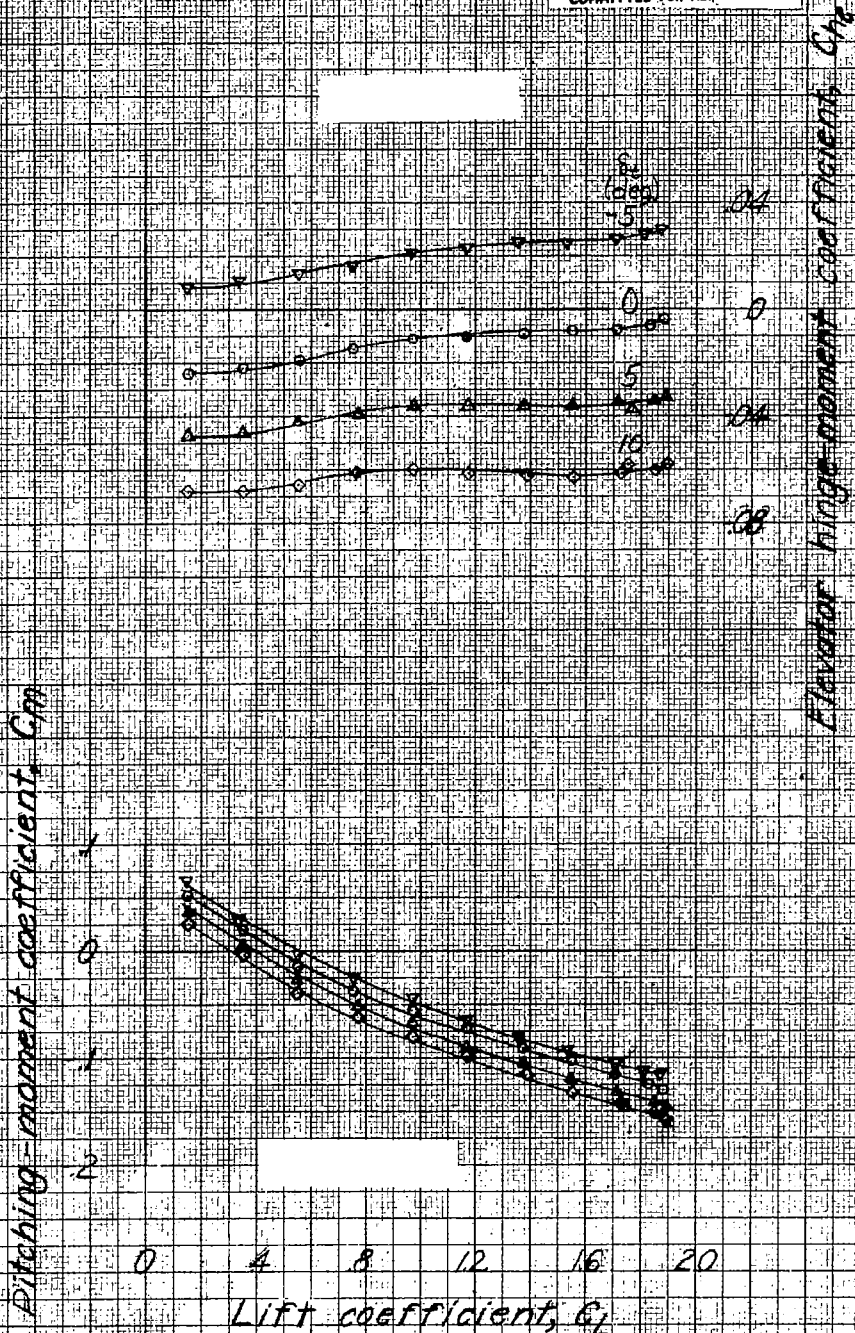
Figure 15- continued

NATIONAL ADVISORY
COMMITTEE FOR AERONAUTICS

Pitching-moment coefficient, C_m

Elevator-hinge-moment coefficient, C_{he}

Lift coefficient, C_L

(d) concluded

Figure 15 - continued

NATIONAL ADVISORY
COMMITTEE FOR AERONAUTICS

(e) Take-off power, landing configuration

Figure 15.- continued

NATIONAL ADVISORY
COMMITTEE FOR AERONAUTICS

(e) concluded

Figure 15.- concluded

Figure 16.- Effect of flap deflection on the aerodynamic characteristics in pitch of the 0.15-scale model of the XBTK-1 airplane. Tail-off, windmilling

α = -6.2°
C_L = -.23

α = 9.0°
C_L = 0.87

α = 12.0°
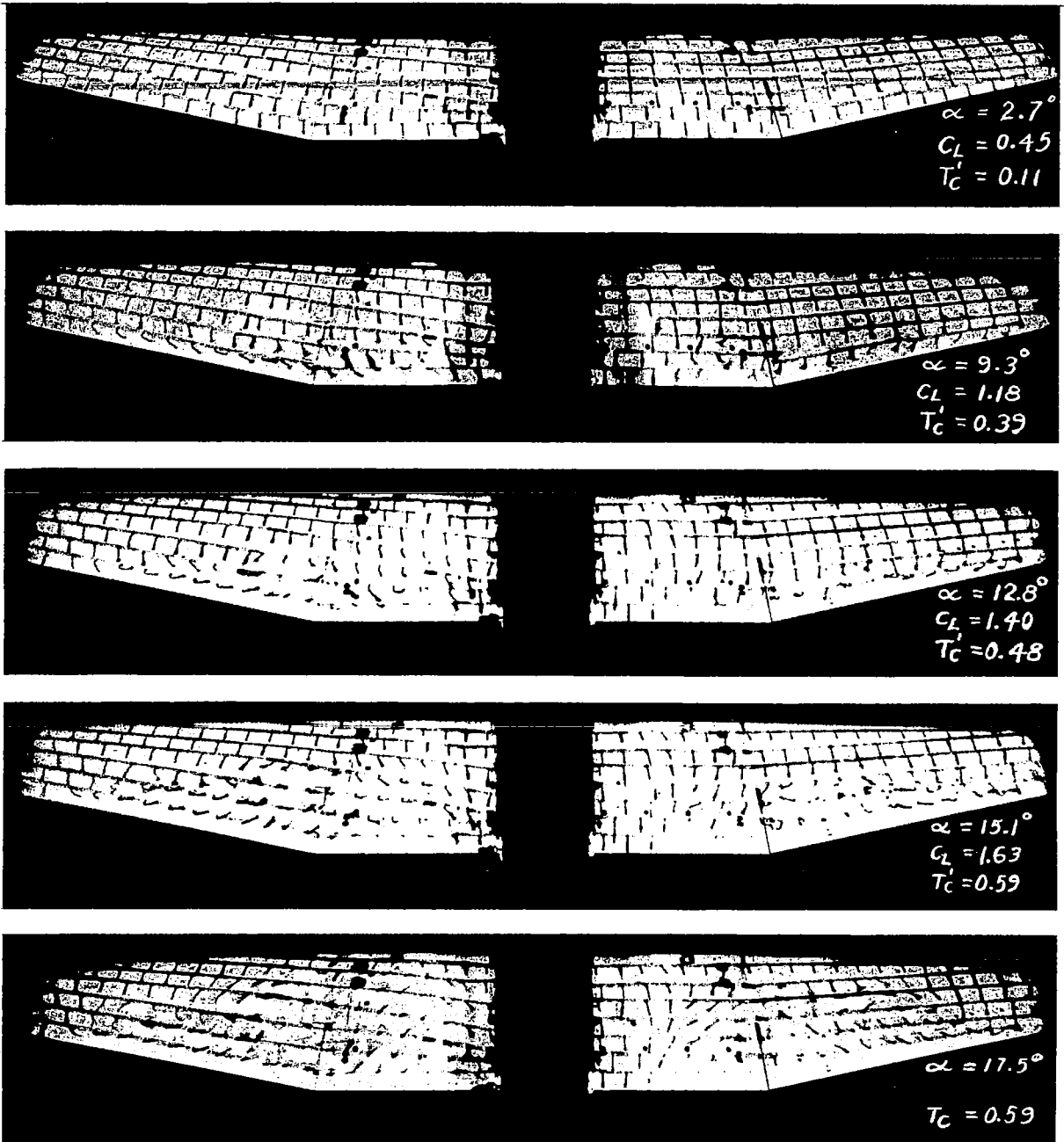C_L = 1.09

α = 14.3°
C_L = 1.27

α = 17.3°
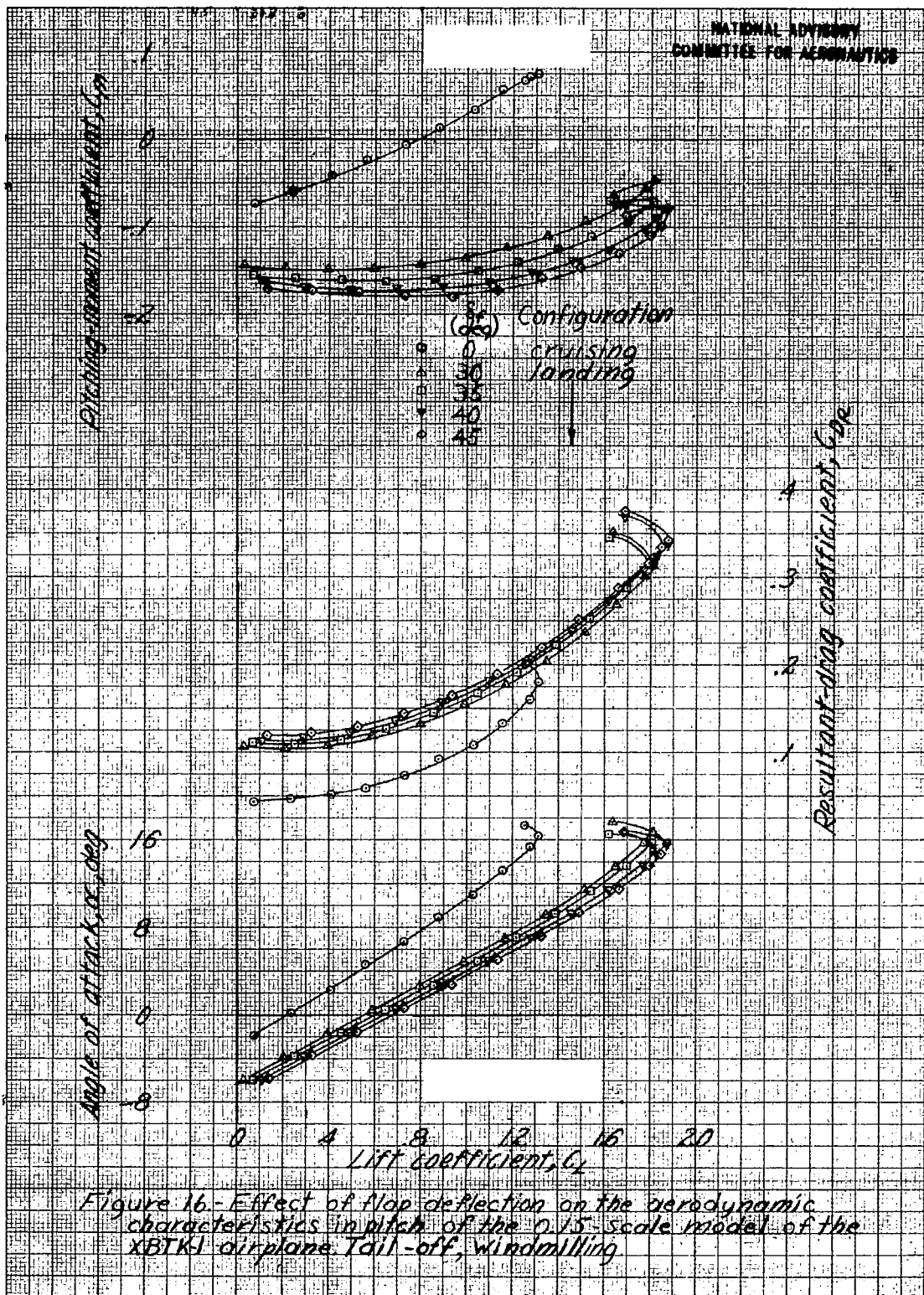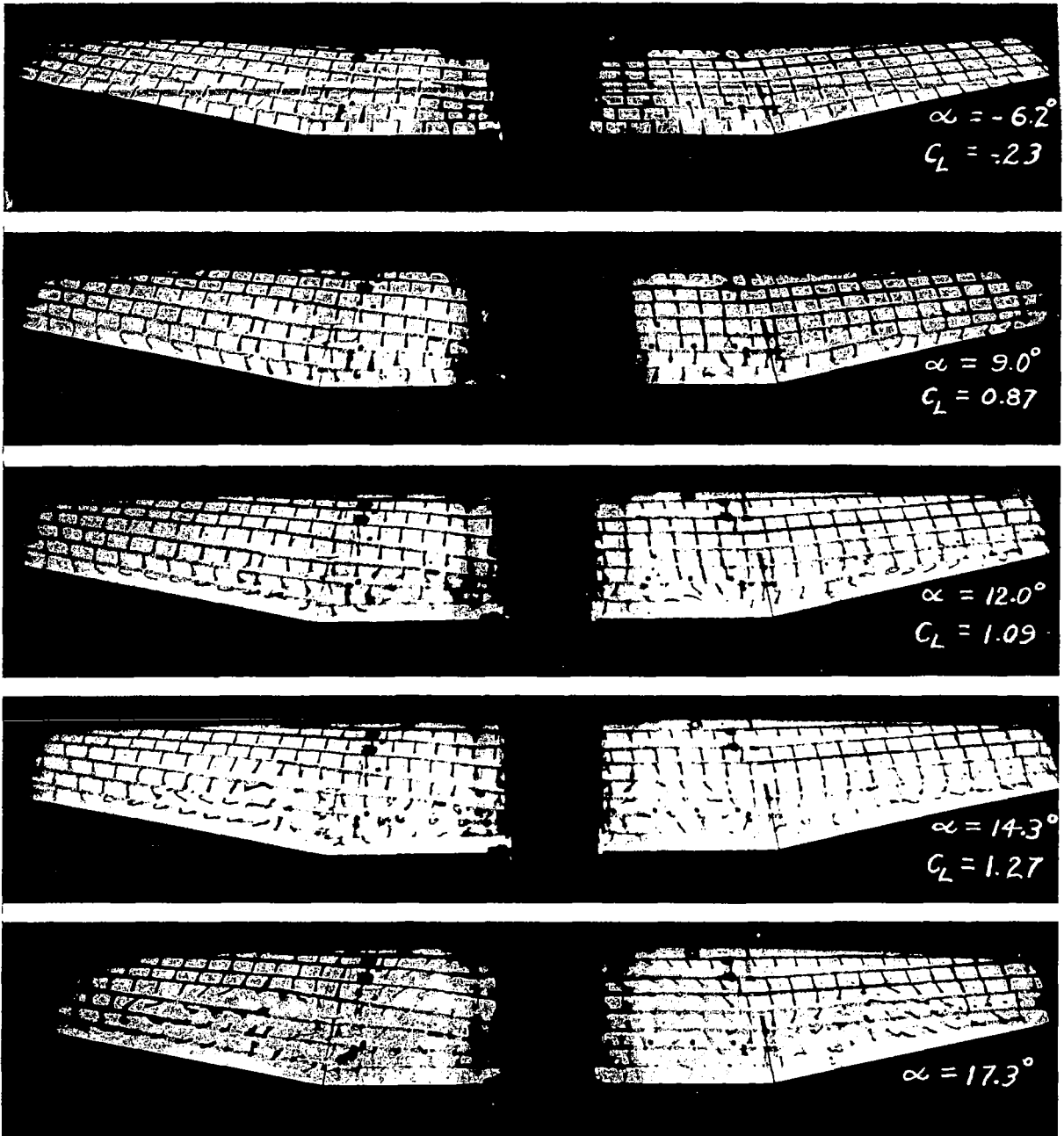
NACA LMAL 41358

Figure 17.- Tuft study of 0.15-scale model of XBTK-1 airplane.
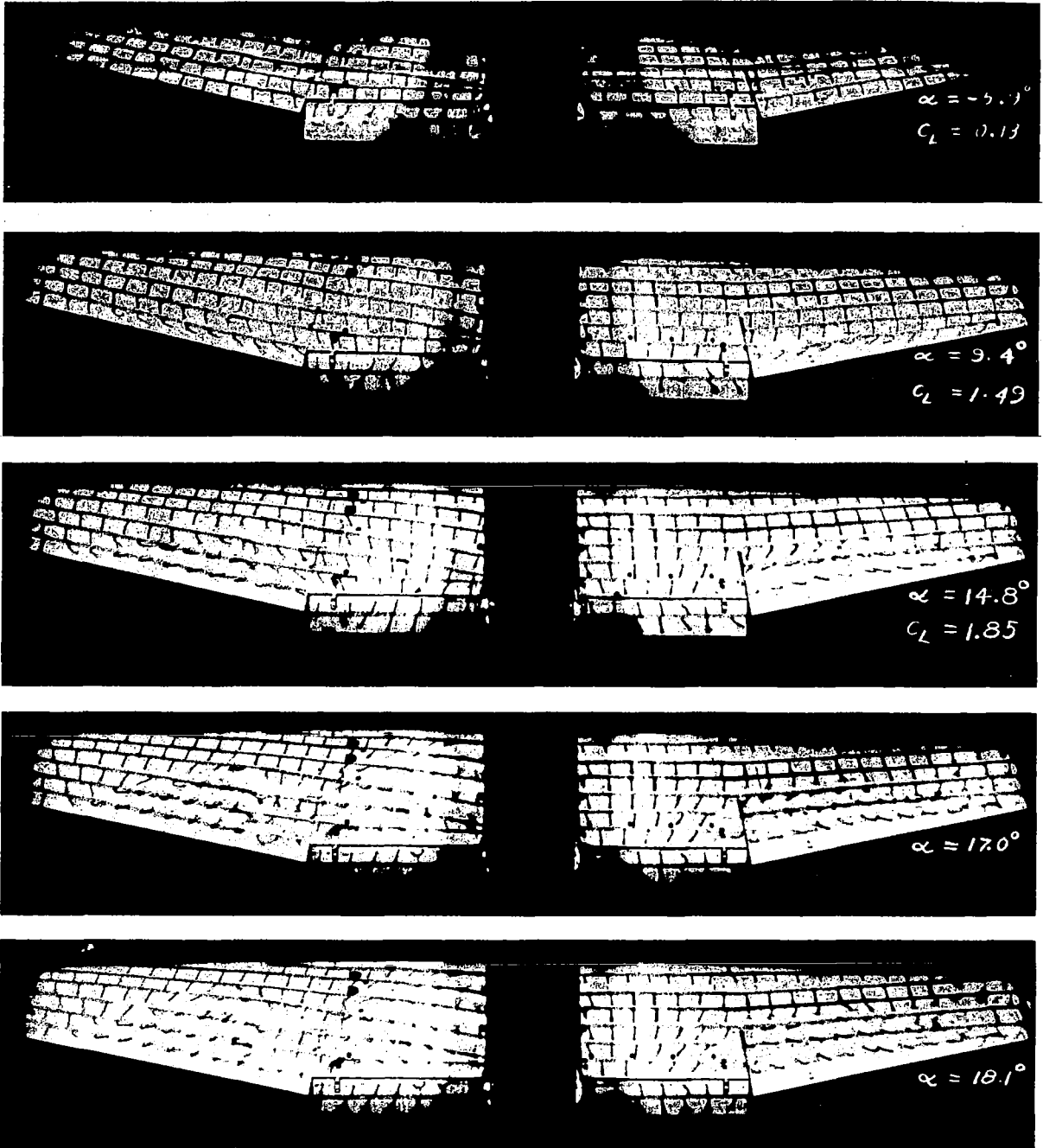Cruising configuration; windmilling; guns, fuel tank and radar
on; tail-off.

α = −6.2°
C_L = −0.23

α = 9 0°
C_L = 0.87

α = 12.0°
C_L = 1.09

α = 14 3°
C_L = 1.27

α = 17.3°
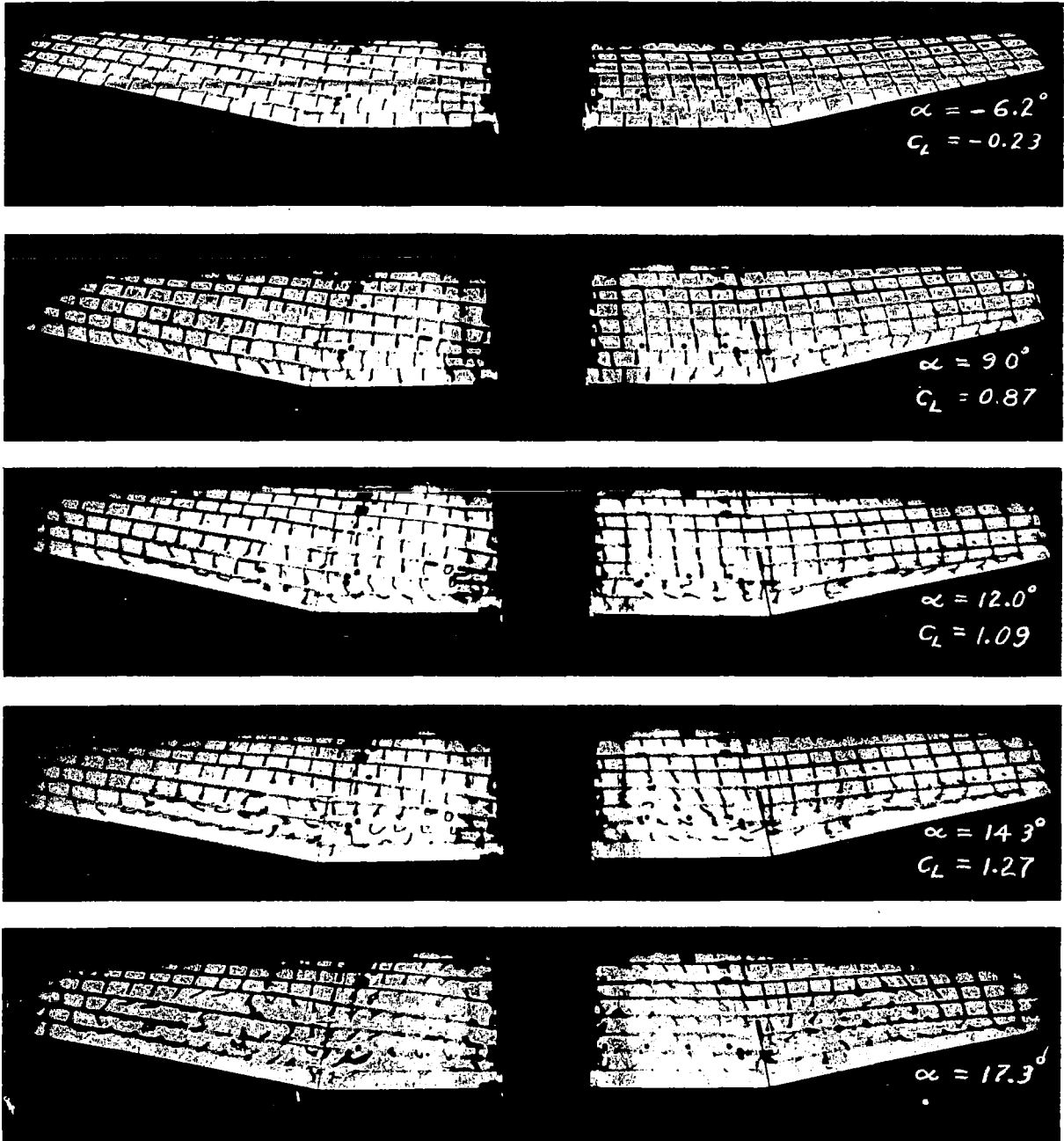
NACA LMAL 41360

Figure 18.-   Tuft study of 0.15-scale model of XBTK-1 airplane.
Cruising configuration; windmilling; guns, fuel tank, and radar
off; tail-off.

$\alpha = 2.7°$
$C_L = 0.45$
$T_c' = 0.11$

$\alpha = 9.3°$
$C_L = 1.18$
$T_c' = 0.39$

$\alpha = 12.8°$
$C_L = 1.40$
$T_c' = 0.48$

$\alpha = 15.1°$
$C_L = 1.63$
$T_c' = 0.59$
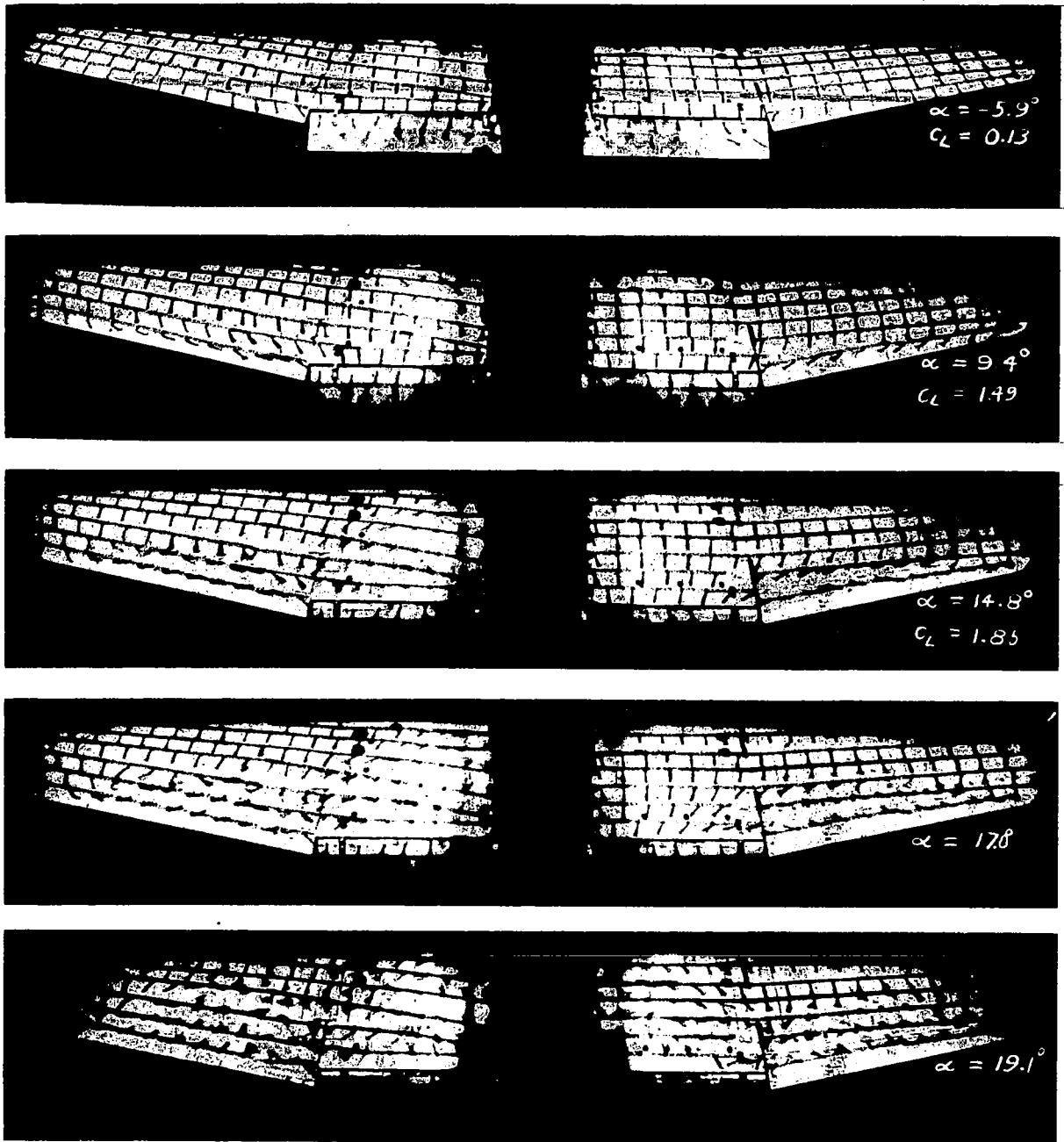
$\alpha = 17.5°$
$T_c = 0.59$

NACA LMAL 41359

Figure 19.- Tuft study of 0.15-scale model of XBTK-1 airplane.
Cruising configuration; take-off power; guns, fuel tank, and
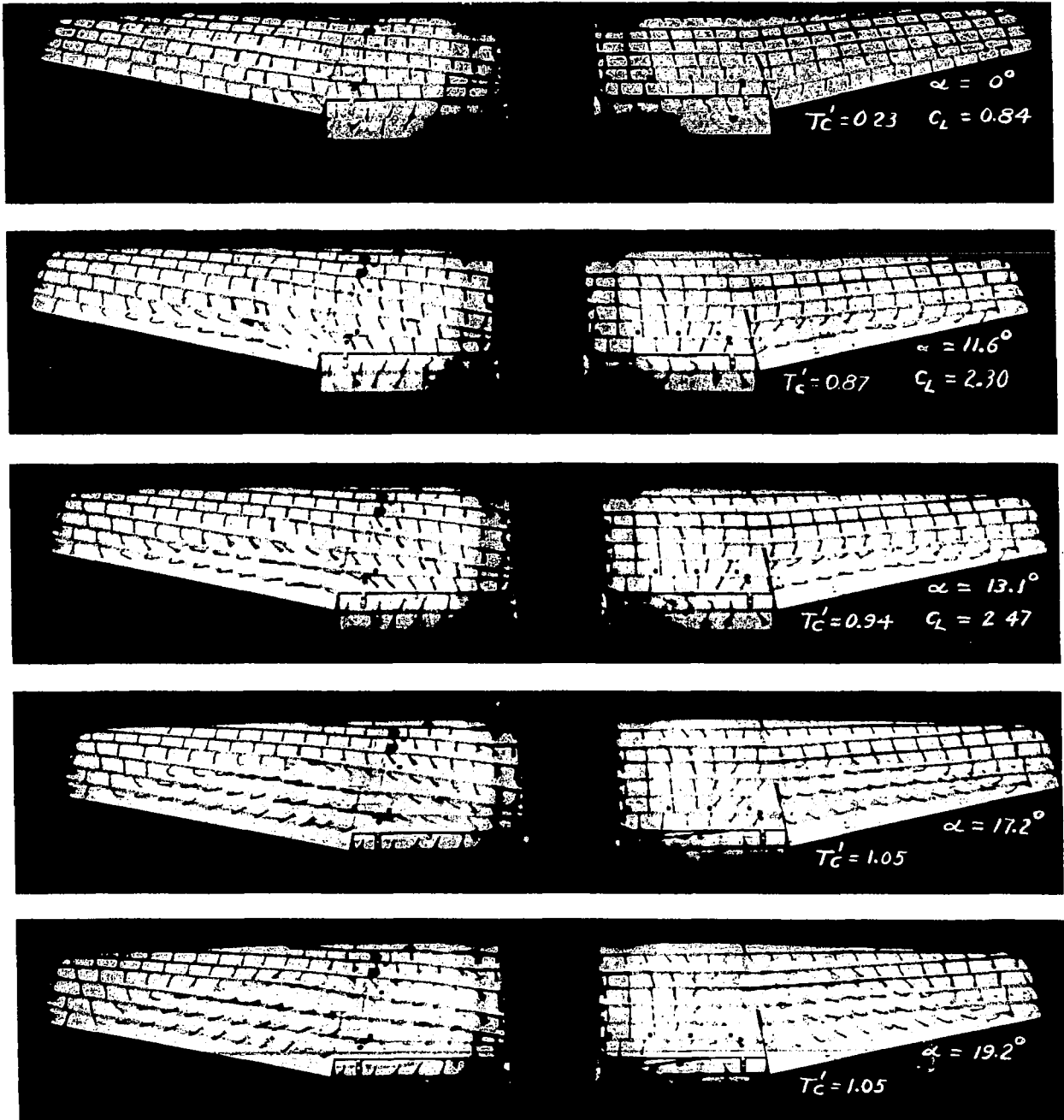radar on; tail-off.

NACA LMAL 41362

Figure 20.- Tuft study of 0.15-scale model of XBTK-1 airplane.
Landing configuration; windmilling; guns, fuel tank, and radar
on, tail-off.

NACA LMAL 41361

Figure 21.- Tuft study of 0.15-scale model of XBTK-1 airplane. Landing configuration; windmilling; guns, fuel tank, and radar off, tail-off.

NACA LMAL 41363

Figure 22.- Tuft study of 0.15-scale model of XBTK-1 airplane.
Landing configuration; take-off power; guns, fuel tank, and
radar on, tail-off.